The Photometric Properties of the *HST* Astrometer Fine Guidance Sensor

B. Bucciarelli[1,2], S. T. Holfeltz[1], M. G. Lattanzi[1,2,3], L. G. Taff[1]
and P. C. Vener-Saavedra[1,4]

Abstract

This paper presents the results of the photometric calibration of the astrometer Fine Guidance Sensor on the Hubble Space Telescope. Dozens of observations of the 9.58 mag Fine Guidance Sensor TRANSfer Mode reference star Upgren 69 (in the cluster NGC 188) have been utilized to verify the consistency and demonstrate the temporal stability of the photo-multipliers. The measurements which provided the material for a transformation from the FGS instrumental system to the Johnson V magnitude consisted of the extensive POSition Mode observations performed during the Optical Field Angle Distortion calibration. A total of 588 measurements of 92 stars in the galactic cluster M35 were performed. Johnson V band photometry with a precision of ± 0.m05 is available with an accuracy of 0.m05 over two years.

I. Introduction

The issues pertinent to the astrometric calibration of the Hubble Space Telescope Fine Guidance Sensors were discussed by Taff (1990a). Unmentioned in that paper was the photometric calibration of the Fine Guidance Sensors (FGSs). While it may seem superfluous to do 1 percent photometry from a space-based platform, in fact the small amplitude variability of one star has already been re-discovered with the astrometer Fine Guidance Sensor (Benedict et al. 1993). Moreover, with the removal of the High Speed Photometer from the *HST* to make room for the Corrective Space Telescope Axial Replacement (COSTAR), the Fine Guidance Sensors, with their 25 milli-second time resolution, become the fastest photometric devices on the observatory. This too has already borne fruit with the observation of a ~ hundred milli-second flare (Benedict et al. 1993). Therefore, there is scientific value to what is a secondary calibration of the FGSs.

Despite the spherical aberration in the primary mirror of the Optical Telescope Assembly (OTA) (Burrows et al. 1991) and the eventual recognition of the fact that each FGS has a unique set of optical and mechanical problems, the photometric performance of the FGSs has apparently not been affected. We believe this to be so because their entrance aperture is 5 x 5 arcsec (albeit degraded as a result of field stop mis-alignments). Moreover, the introduction of COSTAR will not change the

1. Space Telescope Science Institute, Baltimore, MD 21218
2. On leave from Torino Observatory.
3. Affiliated with the Astrophysics Division, Space Science Department, ESA.
4. Now with Advanced Computer Concepts, GSFC.

nature of the wave front received by the FGSs for they are located in radial bays at the perimeter of the focal plane. Hence, the photometric behavior of the FGSs is not expected to change in the foreseeable future. One major change from the original scientific calibration plan for the FGSs is that instead of performing observations designed to calibrate all three, only one FGS (the astrometer) is being scientifically metered. This is the one in radial bay #3 and not the one in radial bay #2, which was the pre-launch expectation. The FGS in radial bay #2 evinces the worst performance with the deformed primary mirror and the pre-COSTAR positioning of the secondary mirror of the OTA. The FGSs in radial bays #1 and #2 will only partake of the general engineering calibrations for the FGSs.

Below we first discuss the stability of the photo-multipliers in the astrometer FGS. After demonstrating ± 0.01 mag level performance over the last year and one-half, we then turn to the photometric calibration of the collective action of the four photo-multipliers in the astrometer FGS. We have used the measurements acquired for completion of the Optical Field Angle Distortion—one of the two principal calibration activities for positional astrometry—to provide the information necessary to construct a photometric calibration of the astrometer FGS. Providing a transformation from the FGS instrumental system to a standard photometric system for each of the photo-multipliers separately is a less interesting task because all four PMTs are always in use. However, the sensitivity and responsivity mis-matches between the two photo-multipliers on each axis of an FGS are of engineering and scientific concern so this issue is addressed herein. Several papers dealing with various aspects of the Fine Guidance Sensors have been published (e.g. Taff 1990b, 1991, Bradley et al. 1991). The reader is directed to them for a discussion of the electro-optical aspects of the Fine Guidance Sensors and their intended engineering and scientific functions. Scientific data reduction for the FGSs is discussed in Lattanzi et al. (1992 and 1993).

II. Stability of the Photo-multipliers

To evaluate the temporal stability of the FGS photo-multipliers we have utilized many measurements of the same star since launch. Because the spherical aberration ruined the anticipated collimation of the OTA, an extended empirical attempt to find the optimal positioning of the secondary mirror was carried out. A series of “Nine Points of Light” tests and “Five Points of Light” tests were conducted during the collimation phases of the *HST* commissioning. The same star, which we refer to as Upgren 69 (Upgren, Mesrobian & Kerridge 1972), has been used for all of them. This star has also been used in various engineering and scientific calibrations (principally TRANSfer Mode). Hence, as a consequence of its frequent observation, this star has become the reference star for FGS TRANSfer Mode observing. This star is apparently single—as far as can be determined from FGS observations—point-like, and unvarying in brightness. From the Upgren et al. reference, its V magnitude is 9.58 and its B – V color index is 0.50. The results for the most recent 1.5 years are summarized in Figure 1.

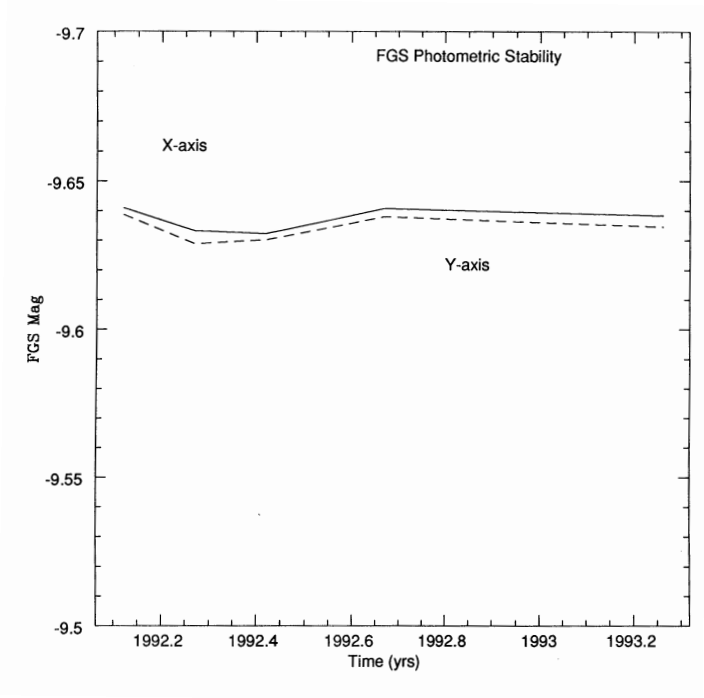

Figure 1: Time history of the astrometer FGS measurements of Upgren 69.

III. Photometric Calibration Data

iii.i Reference Star Data

There is one source of photo-electric photometry of M35 in the literature, Hoag et al. (1961). This work also includes extensive photographic photometry so we adopt it as our reference standard. Additional photographic photometry of this galactic cluster by Cudworth (1971), McNamara & Sekiguchi (1986), and Vidal (1973) was brought onto the Hoag et al. system by the one-dimensional version of the infinitely overlapping circles method (Taff, Bucciarelli & Lattanzi 1990; Bucciarelli, Taff & Lattanzi 1993). To see how this method works to minimize the systematic differences between two different sets of V magnitudes, concentrate on one star in both the Hoag et al. and (say) Cudworth lists. We find all the stars also in this intersection set within $\pm\Delta V(\Delta V = 0.^m33)$ of its V magnitude and store the individual differences $\delta V = V_{Hoag} - V_{Cudworth}$. These are then averaged together with the infinitely overlapping line weight function $w(z)$;

$$w(z) = 1 - z, z = |\delta V|/\Delta V.$$

Thus, the amount of the adjustment is given by

$$\varepsilon_V = \sum w(z)\,\delta V / \sum w(z),$$

where the sums are over all the stars in both the Hoag et al. and the Cudworth data sets and within ΔV of the V magnitude of this star. The re-normalization by the sum of the weights is required because $w(0) \equiv 1$. Thus, the value we use for the V magnitude of this star is $V_{Cudworth} + \varepsilon_V$.

In a similar fashion we separately brought the different B – V values onto the Hoag et al. system (this time with a $0.^m08$ width). Unfortunately, the Cudworth (1971) color indices showed too much dispersion (and residual systematic tendencies) to be successfully merged with the Hoag et al. values. A separate investigation of the B values and the B – V values vs. V was also undertaken to explore the possibility of more subtle systematic problems as a function of color index. No additional causes for rejection or suspicions of inhomogeneity were found at first. All the remaining V and B – V data, adjusted as described, where then used for the photometric calibration of the astrometer FGS. Having minimized the systematic differences, the weight assigned to the photometry was based on the estimates of the random errors assigned by the authors. After this stage of the analysis was completed it became clear to us that the McNamara & Sekiguchi (1986) data had to be rejected because, relative to the FGS instrumental magnitudes, it too showed subtle color index dependent systematic errors. (While the infinitely overlapping circle can remove systematics at any wavelength, it is imprudent to use it on extremely large scales.) Thus, our actual transformation formulas from the FGS instrumental system to the Johnson V magnitude is based on the Hoag et al. (1961) and Vidal data (1973).

iii.ii Observational Data

The Optical Field Angle Distortion calibration (colloquially known as the OFAD) is designed to correct for the residual distortions induced by the combined Optical Telescope Assembly (i.e., the primary and secondary mirrors of the *HST*) and Fine Guidance Sensor optical system aberrations. The observations to support it were successfully carried out over 20 orbits in early January, 1993. Using experience gained from other FGS observing efforts, the Space Telescope Astrometry Team (led by W. H. Jefferys, Univ. of Texas at Austin) was cleverly able to fit in as many as 30 stars per orbit in a complex measurement sequence. Hence, 588 POSition Mode measurements of 92 different stars, in the galactic cluster M35, were obtained.

IV. Numerical Results

iv.i Dead-Time Corrections

The formula for the correction from measured counts (M_C) per unit of integration time (typically 25 msec for the FGSs) to true counts (T_C) is (Hubble Space Telescope Astrometry Operations Handbook 1986, pg. 3-73)

$$T_C/M_C = 1/[1 - M_C(\delta T/\tau)], \quad (1)$$

where δT is the dead-time constant (285 nanoseconds) and τ is the integration time. Equation (1) is expressed on a magnitude scale by taking the common logarithm of the ratio T_C/M_C. Figure 2a shows the amount of correction (in magnitudes) owing to the photo-multiplier dead-time which needs to be applied to the instrumental magnitudes (as derived from the measured counts) as a function of visual (Johnson) magnitude. The absolute throughput (counts) is that for the F583W (Clear) filter. For example, for our standard single star Upgren 69 (V =$9.^m58$) the dead-time correction amounts to 0.09 mag.

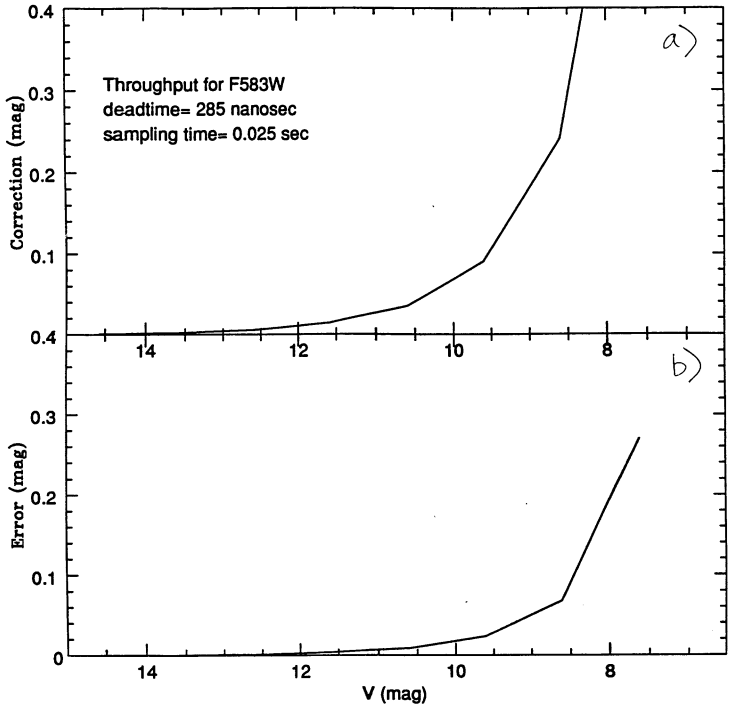

Figure 2: a) Plot of the dead-time correction as a function of V magnitude. b) Graph of the error in the dead-time correction with a 25 percent uncertainty in the dead-time constant.

The dead-time constant just given is based on pre-launch measurements. There has been no in-flight calibration of the dead-time constant either during the Orbital Verification or Science Verification phases of operation. In Eq. (1), the measured counts are known to the limit of the photon noise, while τ is a given number. Thus, an error in the adopted value for the dead-time constant will show as an error in the predicted correction derived from Eq. (1). This error is (in dex)

$$\sigma_{\Delta m} = [2.5\log e \times 10^{0.4\Delta m} M_C(\delta T/\tau)]\,\sigma_{\delta T}/\delta T, \qquad (2)$$

where $\sigma_{\Delta m}$ is the error of the correction Δm as derived from Eq. (1) (after conversion to a magnitude scale) and $\sigma_{\Delta T}$ is the error of the dead-time constant. In Figure 2b we show a plot of Eq. (2) as a function of magnitude for an assumed error in the dead-time constant of 25 percent.

From the two figures we conclude that the dead-time correction is important enough to be routinely removed from the data (and this feature is now built into the Institute's astrometry data processing software). The contribution from our uncertainty in the dead-time constant is several times less than the sought for correction (the actual errors probably being smaller than that depicted in Figure 2b).

iv.ii Linearity

We start out assuming that the relationship between FGS magnitude, m_{fgs}, the mean value of the measured counts, < C >, and color index, B – V, is of the form

$$m_{fgs} = -2.5\log\langle C\rangle, \text{ and } V = -2.5\log\langle C\rangle + \alpha + \beta\,(B-V)\,,$$

where α and β are constants to be determined. In fact, at first we considered a more general model with the numerical factor of 2.5 in the m_{fgs} formula replaced by another constant (say 2.5γ). After extensive testing, not further described herein, we were convinced that the value of this constant was in fact unity ($\gamma = 1.0000 \pm 0.0001$). Hence, we assumed it from that point on.

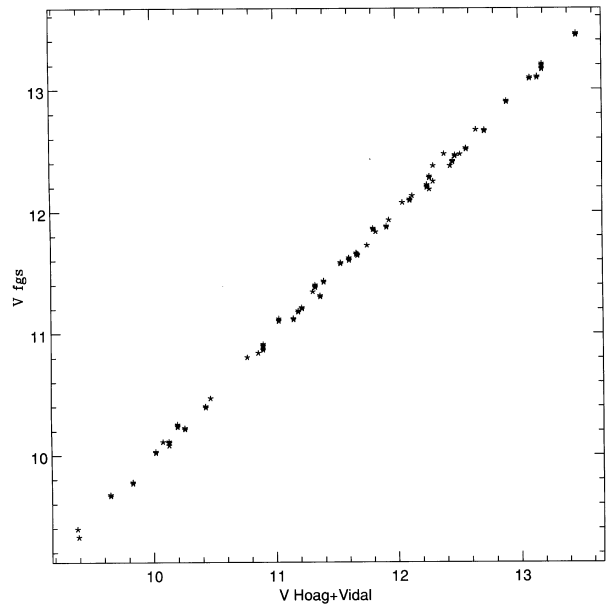

Figure 3: Corrected FGS V magnitude plotted against the standard V magnitude (i.e., the weighted average of the Hoag and Vidal photometry). Note that the 45°, zero intercept line is followed.

Fits [using the GAUSSFIT software (Jefferys 1988)] without the color index term were noticeably poorer than those with it. This is not surprising in view of the wide pass-band of the F583W filter (i.e., 2400Å). Finally, as indicated above, tests of the results after the fit demonstrated that the McNamara & Sekiguichi (1986) data was contaminated by a color index dependent systematic error. Therefore, we eliminated it from our pool of reference data and executed the least squares fits once more relying only on the Hoag et al. (1961) and Vidal (1973) measurements. Graphical results are presented in Figures 3–6. The numerical values of α and β were determined to be 20.060 ± 0.003 and -0.164 ± 0.010 respectively.

From the size of β it is clear that there exists a non-trivial color index dependence in the instrumental FGS magnitude (i.e., in m_{fgs}). However, its amplitude is small and knowing an approximate value of B – V, say even to $\pm 0.^{m}25$, is sufficient to continue to do at least 5 percent photometry.

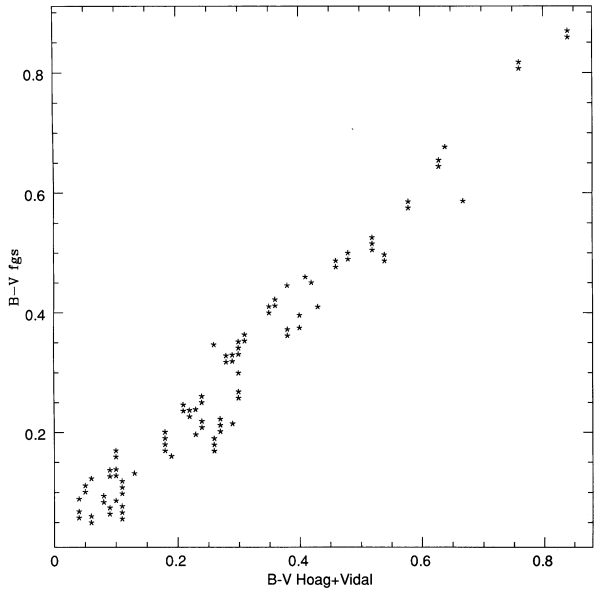

Figure 4: Corrected FGS B – V color index plotted against the standard B – V color index (i.e.,the weighted average of the Hoag and Vidal photometry). Note again that the 45°, zero intercept line is followed.

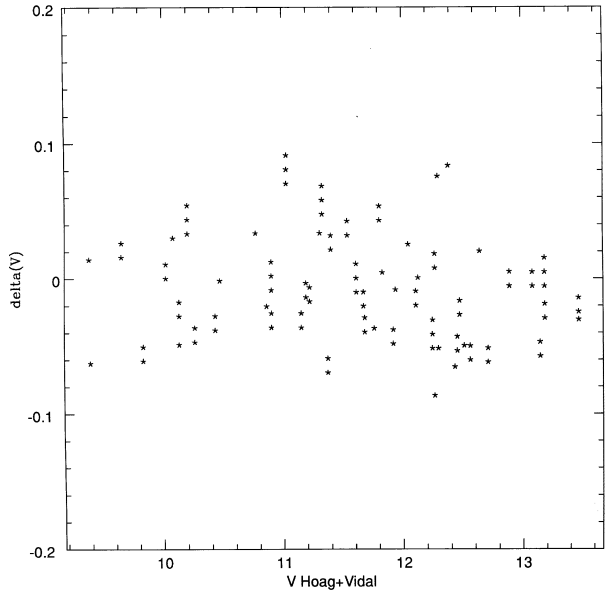

Figure 5: The difference between the FGS V magnitude and the standard V magnitude plotted against the standard V magnitude (i.e., the weighted average of the Hoag and Vidal photometry). Observe that there is no bias and an absence of systematic trends.

iv.iii Photomultiplier Tube Bias per Axis

Using all the observations of the Optical Field Angle Distortion POSition Mode measurements, we have evaluated the differences between the two photo-multipliers per FGS interferometer axis. (These are usually referred to as the x and y axes and the two photo-multipliers as the A and B PMTs.) The results are plotted in Figures 7 and 8. There is evidence of a small color index dependent effect and clearly the two Y axis photo-multipliers are unbalanced.

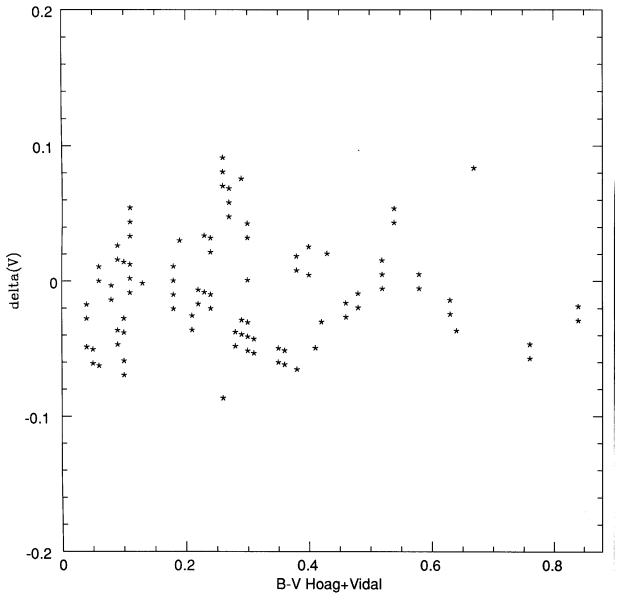

Figure 6: The difference between the FGS V magnitude and the standard V magnitude plotted against the standard B – V color index (i.e., the weighted average of the Hoag and Vidal photometry). Observe again that there is no bias and an absence of convincing systematic trends.

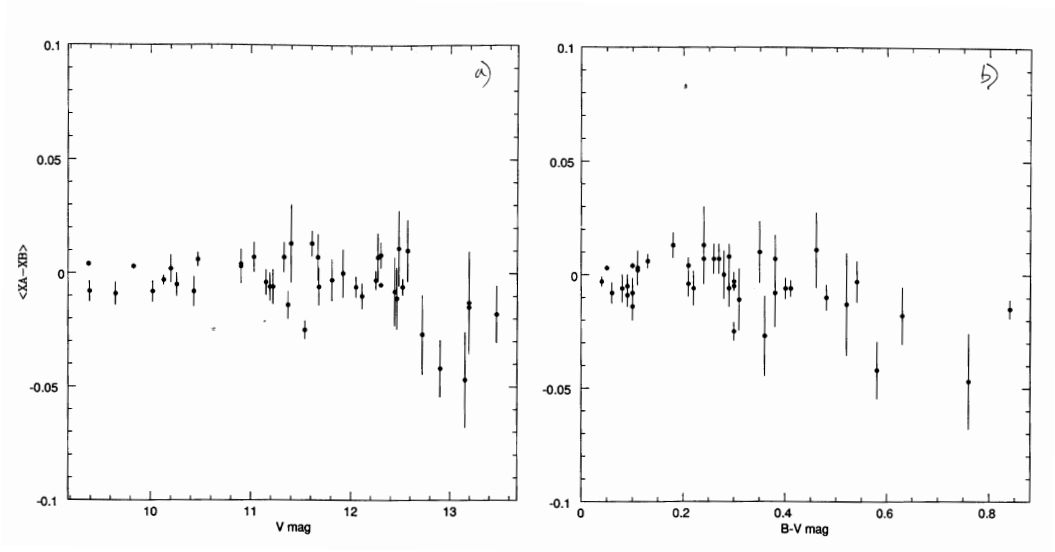

Figure 7: a) X axis count differences, expressed as a magnitude, vs. V magnitude. The error bars indicate the standard deviation about the mean of repeated observations of the same star. b) X axis count differences, expressed as a magnitude, vs. B – V color index, as in Figure 7a.

Conclusions

We have described the methods and material used to ascertain the temporal stability of the astrometer Fine Guidance Sensor photo-multiplier tubes. After satisfying ourselves of this fact we have similarly presented the data and analysis techniques used to photometrically calibrate this device. With a 25 milli-second time resolution, the FGS photo-multipliers are the best means of obtaining fast photometry from *HST*.

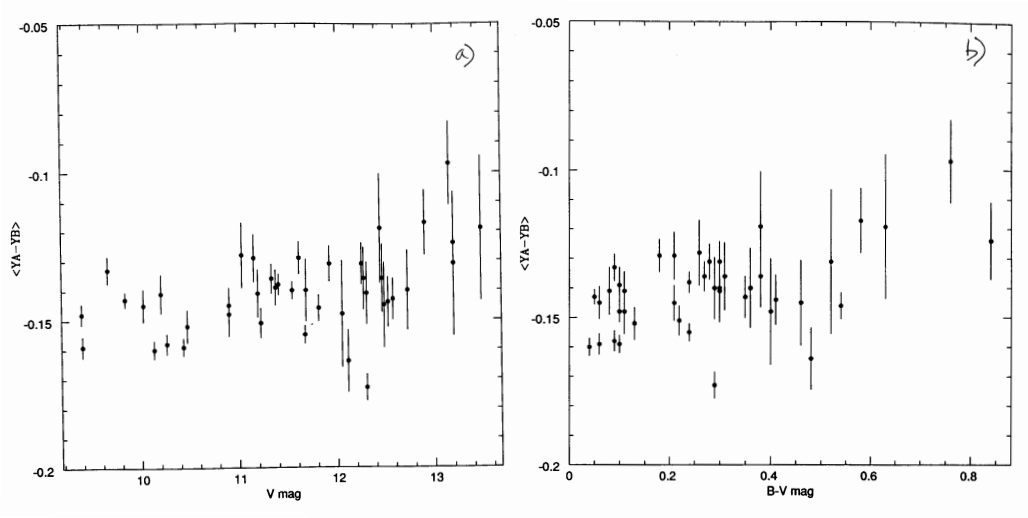

Figure 8: a) Y axis count differences, expressed as a magnitude, vs. V magnitude, as in Figure 7a. Note the non-trivial offset from a null value. b) Y axis count differences, expressed as a magnitude, vs. B – V color index, as in Figure 7a.

This work was partially supported by NASA Grants NAGW-2597 and CW- 0016-92.

References

Benedict, F., E. Nelan, B. McArthur, D. Story, W. van Altena, Yang Ting-gao, W. H. Jefferys, P. D. Hemenway, P. J. Shelus, A.L. Whipple, O. G. Franz, L.W. Fredrick, and R. L. Duncombe, 1993, PASP, 105, 487

Bradley, A., Abramowicz-Reed, L., Story, D., Benedict, G., and Jefferys, W., 1991, PASP 103, 317.

Bucciarelli, B., Taff, L. G., and Lattanzi, M. G., 1993, J. Statist. Comput. Simu. 48, 29

Burrows, C. J., Holtzman, J. A. Faber, S. M. Bely, P. Y., Hasan, H., Lynds, C. R., and Schroeder, D., 1991, ApJ 369, L21

Cudworth, K. M., 1971, AJ 76, 475

Hoag, A. A., Iriarte, B., Johnson, H. L., Hallan, K. L., Mitchell, R. I., and Sharpless, S., 1961, Publ. U. S. Naval Obs. Rep. 17, 349

Jefferys, W. H., Fitzpatrick, M. J., McArthur, B. E. and McCartney, J. E., 1988, GaussFit: A System for Least Squares and Robust Estimation USER'S MANUAL, Version 1.0, (Univ. Texas at Austin, Dept. of Astronomy and McDonald Obs.)

Lattanzi, M. G., Bucciarelli, B., Holfeltz, S. T., and Taff, L. G., 1992, "The Analysis of *HST* Fine Guidance Sensor Transfer Functions," in Complementary Approaches to Double and Multiple Star Research, eds. H. A. McAlister and W. I. Hartkopff, ASP, San Francisco, pg. 377

Lattanzi, M. G., Bucciarelli, B., Holfeltz, S. T., and Taff, L. G., 1993, "Astrometry with the *HST* Fine Guidance Sensors," in Developments in Astrometry and Their Impact on Astrophysics and Geodynamics, eds. I. I. Mueller and B. Kolaczek, Dordrecht, The Netherlands, pg. 47

McNamara, B. and K. Sekiguchi, 1986, AJ 91, 557
Taff, L. G. 1990a, ApJ 365, 407
Taff, L. G. 1990b, Exp. Astr. 1, 237
Taff, L. G. 1991, Adv. Sp. Res. 1, 97
Taff, L. G., Bucciarelli, B., and Lattanzi, M. G., 1990, ApJ 361, 667
Vidal, N. V. 1973, A&A Suppl. 11, 93
Upgren, A. R., Mesrobian, W. S., and Kerridge, S. J., 1972 AJ, 77, 74

Optical Field Angle Distortion Calibration of FGS3

W. Jefferys[1], A. Whipple[1], Q. Wang[1], B. McArthur[1], G. F. Benedict[1], E. Nelan[1]
D. Story[1], and L. Abramowicz-Reed[2]

Abstract

The Hubble Space Telescope carries three Fine Guidance Sensors (FGS) that serve as part of the Pointing Control System and can be used for millisecond of arc astrometry on stars as faint as V=17. The *HST* Ritchey-Chrétien design produces optical distortions in the field of view of the telescope, which because of residual misalignments, must be calibrated on-orbit for any instrument. The method chosen to calibrate these distortions, as they are observed by the FGS, involves exploiting the metric invariance of a rich star cluster with respect to repointing the telescope; that is, the measured relative positions of stars, after calibration, should not depend on where the telescope was pointed. We report the analysis of an extensive series of measurements of the ecliptic open cluster M35, for the purpose of determining distortion polynomial coefficients and other parameters necessary to reduce *HST* astrometric observations with Fine Guidance Sensor 3. Implications for the accuracy of *HST* astrometry are discussed.

I. Introduction

The Hubble Space Telescope is a Cassegrain telescope of the Ritchey-Chrétien design. The prescription of the Optical Telescope Assembly (OTA) contains optical field angle distortion (OFAD) and some astigmatism. Neither coma nor spherical aberration was included in the optical design. The Fine Guidance Sensors (FGS) are optical interferometers that measure pointing changes by means of shearing the wavefront with Koester's prisms. (For details regarding the entire FGS design see Bradley et al. 1991.) Before light strikes the *HST* focal plane it is diverted to an FGS by means of a pick-off mirror. Next in the optical path is an aspheric mirror that corrects for the design astigmatism and almost totally collimates the beam. Following the asphere is a Star Selector composed of two fold flat mirrors and a five element corrector group which rotate as one unit. After the corrector group, the beam is totally collimated. Also, the pupil is located beyond this point (see Figure 1 in Bradley et al. 1991 for the optical layout of the FGS).

The combined OTA/FGS design contains distortion and lateral color effects. Distortion is a field dependent aberration that displaces the true star position but does not degrade image quality. The lateral color displaces the true star position as a function of field location and color temperature of the target. The design distortion

1. Astronomy Department and McDonald Observatory, University of Texas, Austin, Texas 78712
2. Hughes Danbury Optical Systems, Danbury, Connecticut 06810

within the FGS can impart pointing errors as large as 6 arc seconds. Lateral color contributes about 5 mas (worst case) to positional error. Although the design distortion is large, initial estimates for its signature are obtained through raytraces. Hence a substantial amount of design distortion can be removed with pre-launch estimates. Also, the majority of the design distortion results in an effect that mimics a change in the plate scale. The nonlinear distortion is only about 0.5 arc seconds.

The classical telescope design and lateral color are not the only sources of distortion that affect astrometric measurements. Figure errors on optical surfaces that are not near the pupil generate local wavefront tilts. The FGS pick-off, aspheric and Star Selector A fold mirrors are in this category. Figure error in the optical elements that are located beyond the five element corrector group of Star Selector A have no effect on the data, since the beam is totally collimated at that point. Misaligned Star Selector mirrors and clocking offsets between the Star Selectors and their respective encoders also contribute to distortion. Encoder bit errors add both low and high spatial frequency distortions to the target's location. Finally, launch stress, moisture desorption and misaligned optical elements will change the signature of design distortion. Astrometric data must be adjusted for these distortions. Prior to launch these contributors were identified and methods to remove their effects, via on-orbit calibrations or subtraction maps, were devised.

Of course, it is well known that the *HST* OTA design was not realized (Burrows et al., 1991). Due to figure error, the primary mirror has approximately 0.4 waves rms of spherical aberration at 633 nm wavelength. The fact that the figure error is in the primary mirror, and not in the secondary, means that spherical aberration was introduced without the introduction of coma. This is critically important to the operation of the FGS since coma destroys the interference transfer function that is at the heart of the FGS function whereas spherical aberration does not. The spherical aberration does have some detrimental effect on the FGS, however (Ftaclas et al. 1993). This is because residual misalignments of the collimated beam on the Koester prisms cause the spherically aberrated wave front to be sheared by the Koester prism. Since the derivative of spherical aberration is coma, this shearing effect in the FGS mimics coma in the OTA. Fortunately, the amount of coma that has been introduced into the FGS by this mechanism is sufficiently small that it has not destroyed the observability of the transfer functions. But it has introduced an additional source of positional distortions that can and must be calibrated along with the OFAD. This source of distortion appears to be constant for a given secondary mirror position. It has an amplitude of approximately 10 mas and slowly varies across the FGS FOV. For the purposes of the OFAD calibration, the two sources of positional distortion, the optical design and the effect of a misaligned pupil combined with spherical aberration, are inseparable and so they are considered as a single distortion in our analysis.

Two additional sources of difficulty have been discovered since launch. First, for reasons that are not well understood at this time, the metrology of the FGS optical system has not fully stabilized. A post-launch period of change was expected since the metering structures are made of graphite epoxy which shrinks in a non-uniform way due to water desorption. While the amount of change that is observed has dramatically decreased since the first few months after launch, there remains a time varying part of the distortions that are observed by the FGS. We have had to

generalize our model and our calibration tests to account for these time dependent changes. The second source of difficulty that has been encountered is what appears to be short-term changes of the primary-to-secondary mirror despace that results in a focus shift over the *HST* orbit. The Wide Field and Planetary Camera, as well as the FGSs, have observed this phenomenon. It is hypothesized that the change in secondary mirror despace (also known as breathing) is caused by thermal variations during the 90 minute orbit, see Hasan and Burrows this volume. In the astrometry FGS it is predicted that changes in translation, roll and scale of the targets occur during an orbit as a result of the focus change. An effective observing strategy is to revisit three check stars several times over an orbit, in addition to the program stars. From the check star information an affine transformation can be computed that corrects for the effects of breathing. The negative aspect of this scenario is that it reduces the number of program stars that one can observe over the orbit.

Although there are three FGS interferometers on-board *HST*, the large amount of spacecraft time required to fully calibrate each unit led to the decision to designate one FGS as the astrometer and then to fully calibrate only that unit. An extensive set of tests was undertaken and analyzed. These tests resulted in the decision to choose FGS 3 as the astrometer (Benedict et al. 1992). The remainder of this paper deals with the calibration of FGS 3 exclusively.

II. The Determination of OFAD

ii.i. Overlapping plate method

Jefferys (1979) developed an overlapping plate method to determine the OFAD. The telescope would be pointed toward a rich field of stars, such as an open cluster, extending over approximately 30 arc minutes containing many stars with magnitudes ranging from 10 to 14. Measuring a set of stars which appear in the FGS field of view (colloquially known as a pickle because of its shape), we get an observational plate. Then we offset the telescope slightly, and do the measurement again to get another plate. These two plates contain several common stars, but the common stars will appear in different positions of pickle. If there were no distortion effects, the relative star positions from the two plates would be the same. In other words, any positional differences must be caused by distortion due to the measurements being made in different regions of the pickle. By observing many stars on many plates, we can find a model that best fits the data.

The criteria for choosing the total number of plates and the sizes of offsets are:

- the offsets should be large while including as many common stars as possible,
- the calibration should use as few plates as possible, while keeping the precision of the reduction at the desired level, since the observations are quite time-consuming.

After many simulations, we chose a set of 19 pointings as the baseline, which contains a central pointing, six small-offset pointings that are arranged in a hexagon that is 120 arcsec from apex to apex across the center, six larger-offset pointings

whose centers lie on the central radius of the pickle, and six rotated plates that are centered on the central pointing and on each of the middle pair of larger-offset pointings. The rotated plates were rotated as much as the roll constraints on the telescope would permit. For the time that the calibration was run (10 January 1993 UT), the maximum permissible rolls were +30° and –25°. Figure 1 shows the FGS fields of view for the 19 pointings projected onto the calibration star field in M35. The one pickle that is concave up represents the pointing we use during the fall (when the telescope has rolled through 180° due to solar array pointing constraint) to monitor the OFAD.

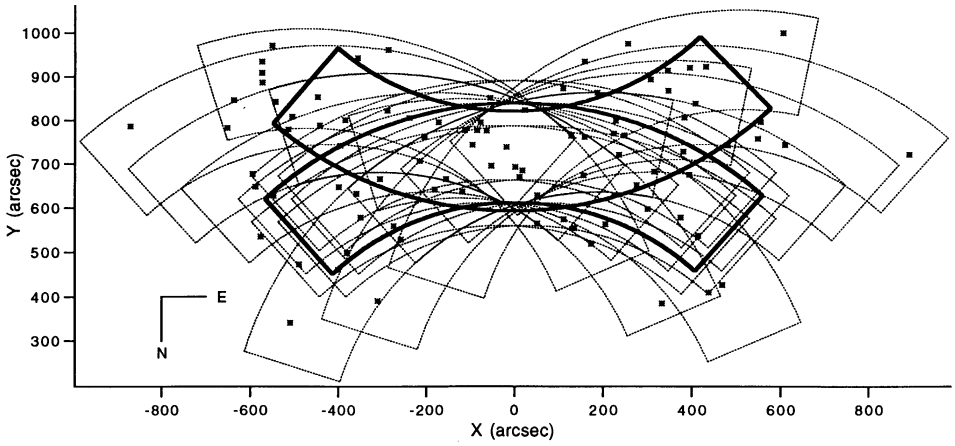

Figure 1: The geometry of the *HST* OFAD calibration. The positions of the stars used in the calibration indicated. The FGS field of view outlines are shown for the 19 successful orbits of the 10 January 1993 UT calibration run (concave down) as well as for the spring (concave down) and fall (concave up) LTSTAB tests.

ii.ii. The OFAD model

The statistical model for the OFAD can be expressed as:

$$Q_p^{\dagger}\hat{\xi}\, Q_p = \hat{x} + \Delta\hat{x} + \hat{\varepsilon} \tag{1}$$

where $\hat{x}$ is the observed position vector; $\hat{\xi}$ is the unknown parameter of star position vector; Q_p is an unknown quaternion for transforming the different plates to the reference plate (Jefferys, 1987); $\Delta\hat{x}$ includes systematic corrections of the pick-off, aspheric collimating, and upper and lower fold flat mirror figure errors, the velocity aberration, the telescope guiding errors, the star selector encoder (SSE) parameters, and the OFAD; $\hat{\varepsilon}$ is the random error (assumed Gaussian). Of the systematic corrections, those due to the pick-off, aspheric collimating, and upper and lower fold flat mirror figure errors, and the velocity aberration are known (in the case of the mirror figure errors, from pre-launch calibrations) and can be corrected as a part of the normal "pipelining" of the data. The remaining corrections due to the unknown (and possibly time dependent) SSE parameters, and the OFAD must be estimated

from on-orbit data. Finally, two sets of "nuisance" parameters must be estimated as well. These account for the pointing and guiding of the telescope during the calibration observations (and, for that matter, during science observations). All of these facets of our OFAD model are detailed below.

ii.iii. The catalogue position

When measuring the position of a star using the FGS, we must first transform its equatorial coordinates *a*, *d* from an existing relatively low-accuracy (~20 mas) star catalogue to the pickle coordinate frame $\hat{\xi}$. Since FGS astrometry involves relative measurements with respect to the V1 axis, we also need to choose a space orientation α_o, δ_o of the V1 axis and a roll angle θ_o around the V1 axis so that the desired star can be found in the pickle. There are several ways to do the coordinate transformation. Here we use the quaternion method developed by Jefferys (1987), in order to maintain consistency with the other parts of the data reduction. We first rotate coordinates from equatorial to the V1 axis frame $\hat{\xi}_s$:

$$\begin{bmatrix} 0 \\ \xi_s \\ \eta_s \\ \zeta_s \end{bmatrix} = Q_{es}^{\dagger} \begin{bmatrix} 0 \\ \cos\alpha\cos\delta \\ \sin\alpha\cos\delta \\ \sin\delta \end{bmatrix} Q_{es} \tag{2}$$

where the quaternion Q_{es} can be expressed as three consecutive rotations

$$Q_{es} = Q_\alpha \cdot Q_\delta \cdot Q_\theta \tag{3}$$

and where $Q_{es}^{\dagger}$ is the conjugate of Q_{es}, and

$$Q_\alpha = \begin{bmatrix} \cos\frac{\alpha_0}{2} \\ 0 \\ 0 \\ \sin\frac{\alpha_0}{2} \end{bmatrix}, \; Q_\delta = \begin{bmatrix} \cos\frac{-\delta_0}{2} \\ 0 \\ \sin\frac{-\delta_0}{2} \\ 0 \end{bmatrix}, \; Q_\theta = \begin{bmatrix} \cos\frac{\theta_0}{2} \\ \sin\frac{\theta_0}{2} \\ 0 \\ 0 \end{bmatrix}. \tag{4}$$

The next step is to transform the coordinates from the V1 axis to the i*th* FGS frame $\hat{\xi}$ that we are using:

$$\hat{\xi} = Q_i^{\dagger}\hat{\xi}_s Q_i \tag{5}$$

where the nominal values of the quaternion Q_i, i =1,2,3 for the three FGSs are:

$$Q_1 = \begin{bmatrix} \frac{\sqrt{2}}{2} \\ 0 \\ \frac{\sqrt{2}}{2} \\ 0 \end{bmatrix}, Q_2 = \begin{bmatrix} \frac{1}{2} \\ -\frac{1}{2} \\ \frac{1}{2} \\ -\frac{1}{2} \end{bmatrix}, Q_3 = \begin{bmatrix} 0 \\ \frac{\sqrt{2}}{2} \\ 0 \\ \frac{\sqrt{2}}{2} \end{bmatrix}. \tag{6}$$

The first component of the quaternion is the “scalar” or “real” part and the other three components comprise the “vector” or “imaginary” part. That is,

$$\begin{bmatrix} a \\ b \\ c \\ d \end{bmatrix} = a + b\hat{i} + c\hat{j} + d\hat{k}$$

with

$$\hat{i}\hat{j} = \hat{k} = -\hat{j}\hat{i}$$

$$\hat{j}\hat{k} = \hat{i} = -\hat{k}\hat{j}$$

$$\hat{k}\hat{i} = \hat{j} = -\hat{i}\hat{k}$$

As it will bear on our results concerning the relative positions of the stars that will be discussed in Section 4, it should be stressed here that the values of α_o, δ_o and θ_o cannot be estimated from the FGS data to a level of accuracy that is any better than the ground-based catalog that is used. Positional astrometry with the *HST*/FGS system is strictly relative, not absolute.

ii.iv. The correction for velocity aberration

Due to the space motion of *HST*, the measured positions will suffer a substantial amount of velocity aberration (about several arc seconds). Murray (1983) gives the relativistic vectorial expression for the aberration $\hat{a}(\hat{x})$:

$$\vec{x}_{true} = \vec{a}(\vec{x}) = \frac{\vec{\vec{L}}(\vec{x} + \vec{\beta})}{1 + \beta \cdot x} \tag{7}$$

where $\vec{\vec{L}}$ is the Lorentz tensor:

$$\vec{\vec{L}} = \frac{\vec{\vec{I}}}{\gamma} + \left(1 - \frac{1}{\gamma}\right)\frac{\hat{v}\hat{v}^T}{v^2} \tag{8}$$

with

$$\gamma = \frac{1}{\sqrt{1 - \beta^2}}; \quad \vec{\beta} = \frac{\vec{v}}{c},$$

where c is the speed of light, and $\vec{v}$ is the space velocity of *HST* in the pickle frame, and v and β are the magnitudes of $\vec{v}$ and $\vec{\beta}$, respectively.

For relative measurements, the main effects of the aberration will cancel, and only the differential aberration is significant at the order of ±20 mas. Here the differential aberration refers to the aberration difference between some reference axis (the direction for which the absolute velocity aberration has been corrected) and the star which we are measuring:

$$\vec{x}_{true} = Q_t^{\dagger}\vec{a}(\vec{x})\,Q_t, \tag{9}$$

where $\vec{x}_{true}$ are the unaberrated coordinates, $\vec{x}$ are the aberrated ones, $\vec{a}(\vec{x})$ is the absolute aberration, and Q_t is the quaternion which rotates the coordinates of the aberrated reference axis to the unaberrated reference axis. Thus the corrections become,

$$\Delta\vec{x}_{aber}(\vec{x};a,e,i,\Omega,\omega,M_0) = \vec{x}_{true} - \vec{x}. \tag{10}$$

To determine the Q_t, we take the *HST* axis that was corrected for absolute velocity aberration as our reference axis, $\vec{x}_{ref}$, which by definition, suffers no differential aberration. Thus,

$$\vec{x}_{ref} = Q_t^{\dagger}\vec{a}(\vec{x}_{ref})\,Q_t. \tag{11}$$

ii.v. Pick-off and aspheric mirror figure error corrections

As with any optical surface, the as-built mirrors in the FGS are not perfect. Misfigured surfaces which are not near the system pupil produce slope (pointing) errors across the full aperture (see Figure 1 in Bradley et al. 1991 for the location of

the pupil). The FGS pick-off and aspheric mirrors are the main contributors to this type of distortion with an amplitude range of 2 to 5 mas. To a lesser extent the Star Selector A fold mirrors add to this effect.

Prior to FGS assembly, each mirror was tested interferometrically. The wavefront tilts, figure error, for individual subapertures were converted to object space distortions. By *HST*/FGS convention, object space refers to a celestial coordinate system that is rotated, but not projected, to be fixed to any of the three FGSs. The distortions were fit to the OFAD polynomial (see Section ii.x for the form of the polynomial). Much of the figure error was characterized by the polynomial. However, there existed locations in FGS FOV that contained high spatial frequencies in figure error. Hence, the residual errors in the polynomial fit were larger at these positions. In order to avoid this effect, the observed FGS data are corrected for the measured errors in the pick-off and aspheric collimating mirrors as part of the normal pipelining of the data.

ii.vi. Encoder errors

The 21 bit optical encoders in the Star Selector Assemblies cause small oscillatory errors in the reported positions due to the inevitable manufacturing imperfections in the encoder masks. These errors are repeatable and were characterized prior to launch. The 14 most significant bits contribute low frequency errors that are readily absorbed by the OFAD calibration. The errors that are associated with the 7 least significant bits have higher frequencies and cannot be accommodated by the OFAD. Consequently, a pre-launch calibration was used to generate a look-up table that is used to remove the least significant bit errors during the processing of the data.

ii.vii. Quaternions as plate constants

Using quaternions as plate constants, we can precisely transform a star vector from a standard plate $\hat{\xi}$ to the measured plate $\hat{x}$ without introducing any approximations (Jefferys, 1987):

$$\hat{x} = Q_p^{\dagger}\hat{\xi}Q_p, \tag{12}$$

where the quaternion Q_p satisfies $Q_p^{\dagger}Q_p = 1$.

ii.viii. Spacecraft jitter and drift correction

The normal function of the two guiding FGSs is to hold the spacecraft pointing fixed such that the guide star in the dominant FGS does not move and to hold the roll of the spacecraft fixed such that the guide star in the sub-dominant FGS is free to move only along the line that passes through it and the dominant guide star. The details of the operation of the Pointing Control System are given in Bradley et al. (1991). For a variety of reasons, the guiding of the telescope during the course of the observations (≈30 minutes) is not perfect at the level of a millisecond of arc. To remove any

residual guiding errors we have implemented a de-jitter algorithm that measures and corrects the instantaneous deviation of the spacecraft pointing from an arbitrary but fixed reference frame. The fixed reference frame is set by the guide star centroids measured during the fine lock interval of the first observation in the plate. For all the other observations in the orbit, any change in the guide star centroids is interpreted as due to vehicle jitter which is then removed from the astrometry star centroid. Specifically, the de-jitter algorithm assumes that any motion of the dominant guide star is due to pure spacecraft translation and that any motion of the sub-dominant star along a direction perpendicular to the line between the guide stars (after spacecraft translation is removed) is vehicle roll.

We have also observed drift of stars in the astrometry FGS relative to the guiding FGSs. This relative motion is thought to be due to a combination of the breathing effect alluded to earlier and thermal effects associated with the FGSs. The solution to this problem is to include in the observation set a series of check stars that are revisited throughout the observation set. For the OFAD calibration, we included three stars in each plate that we observed, in sequence, at the beginning and end of the orbit as well as individually during the central part of the orbit. For example during the observation at the central pointing, the identification numbers, in our numbering system, of the check stars were 862, 853, and 894. Star 862 was observed 1st, 15th, and 30th; star 853 was observed 2nd, 9th, 20th, and 29th, and star 894 was observed 3rd and 28th during the total plate of 30 observations. We used a solid body linear drift model (i.e. FGS 3 was assumed to move as a solid body with constant velocity and no rotation relative to the two guiding FGS units) of the form

$$\Delta\dot{x}_{drift}\left(\dot{x}_i;\dot{\dot{x}}_j\right) = \dot{\dot{x}}_j\,(t_i - t_{1j})\,, \tag{13}$$

where j is the plate number, i is the star number within the jth plate, t_i is the time of the observation, and t_{1j} is the time of the first observation in the jth plate. Note that if there is only one observation of a given star on a particular plate (i.e. the star is not a check star) then the position of that star changes but it does not contribute any information to the estimation of the drift.

ii.ix. The correction to SSE

The correction, $\Delta\dot{x}$, due to incorrect initial values of the SSE parameters is:

$$\Delta\dot{x}_{SSE}\,(\dot{x};\rho_A,\rho_B,k_A,k_B,M) = \dot{x}_{true} - \dot{x}. \tag{14}$$

From Figure 2, we see that the raw data of FGS observation are the measurements of the rotation angles of the two star selectors θ_A, θ_B. The Cartesian coordinates, in object space, $\dot{x}$, are derived by using the initial parameter values which may not be well determined. To include any possible corrections for the SSE, we should first convert the $\dot{x}$ back to θ_A, θ_B using the nominal values, then by letting the parameters vary freely, convert them back to get $\dot{x}_{true}$.

The polar coordinates, ρ and ϕ, of $\dot{x}$ are given by:

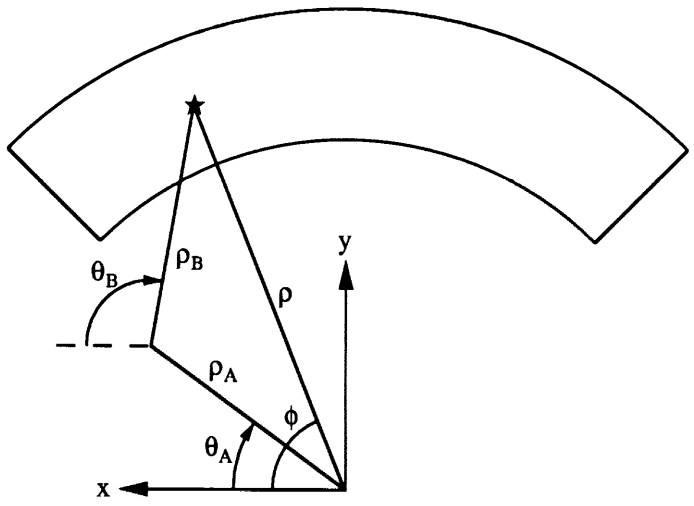

Figure 2: The coordinate system used in *HST* FGS observations.

$$\tan\frac{\rho}{M^o} = \sqrt{\frac{x^2+y^2}{z^2}}$$
$$\tan\phi = \frac{y}{x} \tag{15}$$

and have a spherical trigonometrical relation with θ_A, θ_B (Fresneau, 1985):

$$\cos(180^\circ - q) = \frac{\cos\rho - \cos\rho_A^o\cos\rho_B^o}{\sin\rho_A^o\sin\rho_B^o}$$
$$\cos p = \frac{\cos\rho_B^o\sin\rho_A^o - \sin\rho_B^o\cos\rho_A^o\cos(180^\circ - q)}{\sin\rho} \tag{16}$$

with $\theta_A = \phi - k_A^o - p$ and $\theta_B = q - k_B^o + (\theta_A + k_A^o)$, where the nominal values of the SSE parameters are: $M^o = 57.3$; $\rho_A^o = \rho_B^o = 6.7758^\circ$; $k_A^o = k_B^o = 0$.

Now we transform the raw θ_A, θ_B back to $\grave{x}_{true}$ using the free parameters ρ_A, ρ_B, k_A, k_B and M:

$$\begin{aligned}
\cos\rho' &= \cos\rho_A\cos\rho_B + \sin\rho_A\sin\rho_B\cos(180^\circ - q) \\
\sin\rho'\sin p &= \sin\rho_B\sin(180^\circ - q) \\
\sin\rho'\cos p &= \cos\rho_B\sin\rho_A - \sin\rho_B\cos\rho_A\cos(180^\circ - q)
\end{aligned} \tag{17}$$

with $q = (\theta_B + k_B) - (\theta_A + k_A)$ and $p = \phi' - \theta_A - k_A$. Converting ρ', ϕ' to rectangular coordinates, we obtain $\grave{x}_{true}$:

$$\begin{aligned}
x_{true} &= \sin\frac{\rho'}{M}\cos\phi' \\
y_{true} &= \sin\frac{\rho'}{M}\sin\phi'
\end{aligned} \tag{18}$$

ii.x. The correction for OFAD

We may reasonably represent the OFAD correction by two low-order polynomials in the pickle frame:

$$\begin{aligned}
\Delta x_{dist}(x,y;a_{ij}) &= x_{true} - x = \sum_{i=0}^{5}\sum_{j=0}^{5} a_{ij}x^i y^j \\
\Delta y_{dist}(x,y;b_{ij}) &= y_{true} - y = \sum_{i=0}^{5}\sum_{j=0}^{5} b_{ij}x^i y^j
\end{aligned} \tag{19}$$

where a_{ij}, b_{ij} are a set of constant coefficients to be determined. The actual functional form of the polynomial used is somewhat different. The largest distortion, contributed by the classical design of the aligned powered elements in the OTA/FGS system, has a well-known signature. It is a simple 5th order polynomial that is a function of the sine of the optical field angle, ρ (the radial component of Eq. 18):

$$\Delta_{dist} = \sin\rho_{true} - \sin\rho = a(\sin\rho)^3 + b(\sin\rho)^5. \tag{20}$$

In Cartesian coordinates, this design distortion is cast into the form:

$$\Delta x_{dist}(x,y;a,b) = x_{true} - x = ax(x^2+y^2) + bx(x^2+y^2)^2$$

$$\Delta y_{dist}(x,y;c,d) = y_{true} - y = cy(x^2+y^2) + dy(x^2+y^2)^2 \tag{21}$$

Misaligned optical elements break the symmetry, add a DC bias, add distortion, and require additional terms in the polynomial. The equations that are actually used for our modeling of the OFAD are:

$$\begin{aligned}\Delta x_{dist}(x,y;a_{ij}) = x_{true} - x = {} & a_{00} + a_{10}x + a_{01}y + a_{20}x^2 + a_{11}xy + a_{30}x(x^2+y^2) \\ & + a_{21}x(x^2-y^2) + a_{12}y(y^2-x^2) + a_{03}y(y^2+x^2) \\ & + a_{50}x(x^2+y^2)^2 + a_{41}y(y^2+x^2)^2 + a_{32}x(x^4-y^4) \\ & + a_{23}y(y^4-x^4) + a_{14}x(x^2-y^2)^2 + a_{05}y(y^2-x^2)^2\end{aligned}$$

$$\begin{aligned}\Delta y_{dist}(x,y;b_{ij}) = y_{true} - y = {} & b_{00} + b_{10}x + b_{01}y + b_{20}x^2 + b_{11}xy + b_{30}x(x^2+y^2) \\ & + b_{21}x(x^2-y^2) + b_{12}y(y^2-x^2) + b_{03}y(y^2+x^2) \\ & + b_{50}x(x^2+y^2)^2 + b_{41}y(y^2+x^2)^2 + b_{32}x(x^4-y^4) \\ & + b_{23}y(y^4-x^4) + b_{14}x(x^2-y^2)^2 + b_{05}y(y^2-x^2)^2\end{aligned} \tag{22}$$

where the coefficients a_{ij}, b_{ij} are the constants that are estimated. From Eq.(22), we can see that the variables x and y are mixed together and both have their own observation errors. This is the errors-in-variables problem which has been discussed by Jefferys (1990).

ii.xi. The constraints

There is insufficient information in the *HST* observations alone to permit the adjustment of the full set of SSE parameters, M, ρ_A, ρ_B, and k_B. Without additional information, the least-squares problem would be singular and the iteration procedure would diverge. So, we introduce an external source of scale information, such as a ground-based catalog, and constrain the estimated scale to approximate the implicit scale of the ground-based catalog. Moreover, our *a priori* knowledge of the plate scale is quite good (approximately one part in 1000) so that we can start the least-squares estimation quite close to the best-fit solution.

In addition to the above constraint, we still have to consider other constraints to arrive at a unique result, due to the fact that we do not want the linear terms in the distortion correction to introduce any additional translation, rotation or scale change. To make this clear, we express our model explicitly in terms of plate constants:

$$\begin{aligned} a\xi + b\eta + c &= x - \Delta x_{dist}(x,y;a_{ij}) - \Delta x\,(M,\rho_A,\rho_B,k_B) \\ -b\xi + a\eta + d &= y - \Delta y_{dist}(x,y;b_{ij}) - \Delta y\,(M,\rho_A,\rho_B,k_B) \end{aligned} \tag{23}$$

The constant and linear terms in the distortion are mixed with a, b, c, d of the plate constants. So we apply the following gauge constraints:

$$a_{00} = b_{00} = 0;\ a_{10} = b_{01};\ a_{01} = b_{10} = 0, \tag{24}$$

to separate the distortion coefficients from the plate constants. The ability to include arbitrary equality constraints is a feature of the GaussFit program we used to implement our algorithm (Jefferys et al. 1988).

Finally, since there is a linear relationship between θ_A, θ_B, k_A, and k_B, only one clocking error, k_A, is estimated. The value of k_B is constrained to be zero.

ii.xii. The condition equations

Let l be the number of stars observed, n be the number of observations in each plate, and m be the number of the plates. The total number of unknowns involved in the model is the sum of: four quaternion components for each plate ($4m$), two drift parameters for each plate ($2m$), a variable number ($\approx$30) of distortion coefficients a_{ij}, b_{ij}, the star-selector-deviation parameters ρ_A, ρ_B, k_A, and two components of star position for each star (2l).

The OFAD is solvable if the total number of the equations is larger than the number of unknowns. Let us roughly estimate these two numbers: suppose we have m=20 plates, each of which contains n=30 observations. The total number of equations is $2mn$=1200. Because of the overlapping plates, every star is observed on at least two plates. In fact, if a star were observed on only one plate it would not contribute any information to the OFAD determination. As designed, the calibration in M35 required the estimation of the positions of l=93 stars. So the number of expected unknowns was approximately $4m+2m+30+3+2l$ = 339 and the least squares problem was well determined.

III. The *HST* Observations

The OFAD calibration actually began in December 1990 with the first of a series of mini-OFADs that were performed to improve the knowledge of the FGS-to-FGS alignments as well as the observed distortions. These calibrations were made to support the general operation of the spacecraft and differed from the full-OFAD calibration in that the positions of the stars were assumed to be known at the 10's of

milliseconds of arc level and were held fixed in the estimation. This simplification meant that the mini-OFAD calibrations required far less telescope time than the full-OFAD (typically a few orbits as opposed to 20). The mini-OFAD calibrations not only succeeded in providing the information needed to accurately point to targets with the small apertures in the other science instruments, but it also revealed time dependent changes in the OFAD. The observations were not of sufficient quality, nor were they made often enough (6 to 12 months was typical of the time between mini-OFADs) to fully resolve the nature of these changes but it appeared that the changes could be modeled, to the accuracy of the data, by a time dependent change in ρ_A.

This discovery prompted us to begin a series of long-term stability tests (LTSTAB for short) to monitor any changes in the OFAD. The monitoring effort consists of periodic visits (ideally once per month) to the M35 field used for the OFAD. In fact, M35 was chosen for the OFAD calibration because of the need to run the LTSTAB tests. Since M35 is in the ecliptic, the telescope does not gradually roll about this field throughout the year as it does for a target off the ecliptic. Instead, the telescope flips 180° when M35 gets closest to the anti-solar point (to be precise, the telescope rolls 180° between December 20 and December 28 with the bulk of the roll occurring on December 24). This means that we can observe the calibration field at two fixed orientations; one in the fall and one in the spring. This maximizes our sensitivity to real changes in the OFAD and minimizes our sensitivity to uncertainties in the OFAD that might appear as changes if the telescope gradually rolled through the calibration field. Each spring the LTSTAB test consists of a single orbit of observations that repeat the central pointing of the OFAD. The fall LTSTAB tests also consist of a single orbit of observations but are rolled approximately 180° about the central pointing of the OFAD calibration. These two pointings are highlighted by the heavy lines in Figure 1. Two executions of the LTSTAB test were made before the OFAD calibration; on December 2 and 14, and three were run after the OFAD calibration; on April 5, 18, and 19. We expect to continue the LTSTAB tests, at a rate of approximately once per month, whenever M35 is observable.

The analysis presented in this report concerns only the 20 orbit OFAD calibration executed on 10 January 1993. The analysis of the OFAD plus LTSTAB data (what has come to be called a grand-OFAD) is still in progress. The preliminary conclusion of that analysis is that the changes that are occurring in the OFAD are of sufficiently low frequency that they can be modeled by changes in the SSE parameters. Consequently, it is meaningful to establish a baseline OFAD calibration from the 10 January 1993 spacecraft run. That is the purpose of this report. Subsequent reports by us will provide the means to model the time changing OFAD, for example by osculating SSE parameters or by a time dependent model and coefficients for the SSE parameters. We do not expect to have to change the coefficients of the 5th order OFAD polynomial.

The OFAD calibration itself occurred over 33 hours beginning on 10 January 1993. The calibration test consisted of 20 orbits. The central pointing was repeated on orbits 2 and 20 to permit us to monitor the stability of the OFAD over this period. The data from orbits 16 (one of the middle-sized large offsets at the nominal roll) and 20 were severely corrupted by problems with the spacecraft guiding. Fortunately, the de-jitter algorithm described in Sec. ii.viii completely recovered the data from orbit 16. It may be possible to recover the data from orbit 20 but they have not been

included in the analysis presented in this paper. On the whole, the telescope guiding was extremely good and a total of 525 observations (out of a possible 540) of 91 stars (out of a possible 93) were usable.

IV. Results from our Analysis of the OFAD Data

We have subjected the data from the 19 uncorrupted orbits from the OFAD calibration run in January 1993 to the analysis described in Section 2. We estimated the relative positions of the stars, the SSE parameters M, ρ_A, ρ_B and k_A, and the OFAD coefficients a_{ij} and b_{ij} simultaneously. Of course, in addition, the nuisance parameters of the plate quaternions and the drift parameters were estimated for each orbit.

TABLE 1. Estimated OFAD parameters for Hubble Space Telescope Fine Guidance Sensor Number 3. The meaning of the parameters is explained in the text. The columns labeled with σ's are the estimated variances of the parameters from the least squares solution. Parameters with zero variance were held fixed. The units for the coefficients a_{ij} and b_{ij} are arcseconds, the units for ρ_A, ρ_B, k_A, and k_B are degrees. The magnification, M, is dimensionless. All values are given with more figures than are significant to avoid truncation errors in the evaluation of the series.

i	j	a_{ij}	b_{ij}	σ_a	σ_b
0	0	0	0	0	0
1	0	-3.45958E-06	0	0	0
0	1	0	-7.59297E-06	0	0
2	0	-0.12955214	0.36034647	0.013	0.073
1	1	0.533394636	-0.050252249	0.27	0.042
0	2	-0.129174425	0.932529323	0.029	0.19
3	0	-486.7902615	21.6245827	33	6.9
2	1	44.18062474	-7.483542931	32	3.3
1	2	-12.75565183	-12.48193571	1.3	14
0	3	21.75969958	-632.8467698	6.6	32
5	0	1757942.554	0	3.4E+05	0
4	1	0	4380733.583	0	3.9E+05
3	2	-113432.3267	0	5.6E+05	0
2	3	0	600275.9563	0	3.3E+05
1	4	505077.8006	0	2.5E+05	0
0	5	0	-387380.1344	0	1.6E+05

		σ
ρ_A	6.90375608	0.010
ρ_B	6.90184945	0.010
k_A	-0.6767212	0.0094
k_B	0	0
M	57.3573493	0.086

The estimated values of the SSE parameters and the OFAD coefficients a_{ij} and b_{ij} are given in Table 1 along with the formal variances, from the least squares estimation, for each. The nonlinear part of the OFAD distortions are shown in Figure 3. Since the OFAD calibration is insensitive to absolute scale, the variances of all scale-like quantities, such as M and ρ_A, are inherently large. The rms of the residuals from the 548 individual observations from the OFAD orbits are 2.3 mas along both the x and y axes. This corresponds to an RSS error in a single observation of 3.2 mas over the entire field of view of the FGS. This is very close to the pre-launch expectation of 2.7 mas.

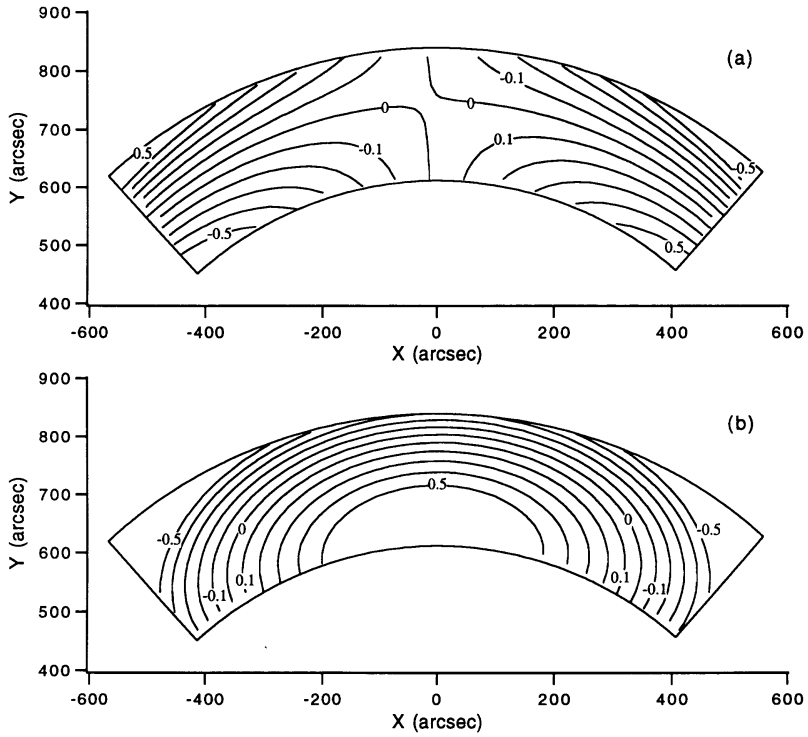

Figure 3: The nonlinear optical field angle distortions due to the *HST* optical telescope assembly as it is convolved with FGS number 3. The contours are labeled with the amount of distortion, in arcseconds, in the x (a) and y (b) coordinates.

It has already been stated that, since there is no field of stars whose relative positions are known to the level of accuracy required for the *HST* OFAD calibration, we have had to estimate the star positions simultaneously. This means that we have the first catalog of relative star positions that are accurate to about 2 mas. Of course, the absolute positions of these stars are only known to the accuracy of the ground-based catalog to which we have referenced the relative positions. For this we used an updated version of McNamara and Sekiguchi's (1986) catalog. Our catalog of 91 stars in M35 is summarized in Table 2. We have tabulated values for the absolute right ascension, declination, and the V magnitude purely for reference and identification purposes. The new results being presented here are the relative coordinates x and h which are given with their estimated variances which were derived from the bootstrap analysis that is described in the next section.

V. Bootstrap Analysis of Bias and Variance

v.i. The definition of bias

The OFAD model Eq. (22) is nonlinear, and nonlinear least squares solutions may be affected by bias. Bias is defined as the difference between the *true T* and the expectation of the *estimated* values *R* of parameters:

$$Bias = E(R) - T \tag{25}$$

The causes of bias may be due to:

- use of the normal assumption when noise is not normal,
- nonlinearities in the model,
- neglect of important systematic effects.

In many practical cases, it is impossible to make the same observations many times to get the mean of solution $E(R)$. Furthermore, we don't know the true values (that's what we want to estimate). Therefore the usual least squares method cannot give a bias estimation.

v.ii. The bootstrap method

Efron's bootstrap method can be used to estimate bias due to causes (1) and (2) (Efron 1982, Wang 1990). The basic idea is as follows:

1. Estimate OFAD parameters $\hat{\theta}$ from the actual data by ordinary least squares fitting. Denote this reference solution as R.

2. Construct an observed-minus-calculated ($O - C$) residual bank from the R solution:

$$r = (O - C) = y - \hat{y} = -Bias + e, \text{ with } E(e) = 0 \tag{26}$$

3. Resample a new set of "observational" data by randomly drawing r from the residual bank with replacement:

$$Y^* = \hat{y} + r = y + e', \text{ with } E(e') = 0 \tag{27}$$

so Y^* is expected to have a bias with respect to the R solution.

4. Estimate the parameter θ again using the same OFAD model:

$$\hat{\theta}^* = \hat{\theta} + Bias + e^*, \text{ with } E(e^*) = 0 \tag{28}$$

Denote the bootstrap solution $\hat{\theta}^*$ as B.

5. Repeating steps (3) and (4) with independent samples a large number of times N, we get the sample mean $E(B)$. The estimate of the bias becomes:

$$\hat{Bias} = E(B) - R \tag{29}$$

From the basic bootstrap assumption $\hat{Bias} \approx Bias$, we equate Eq. (25) to Eq. (29), and obtain the bias-corrected parameter:

$$\hat{T} = R - (E(B) - R) . \tag{30}$$

It follows that

$$E(\hat{T} - T)^2 \approx \sigma_R^2 < E(R - T)^2 \approx \sigma_R^2 + E(Bias)^2 \tag{31}$$

This formula is the basis for our bootstrap analysis.

vii.iii. Checking the assumptions

For practical applications, we use the sample mean and variance to approximate the expectation and variance:

$$E(B) \approx \bar{B} = \frac{1}{N}\sum_{k=1}^{N} B_k, \tag{32}$$

$$\sigma_B \approx \hat{\sigma}_B = \sqrt{\frac{1}{N-1}\sum_{k=1}^{N}(B_k - \bar{B})^2}, \tag{33}$$

$$\sigma_{\bar{B}} = \sqrt{\frac{1}{N(N-1)}\sum_{k=1}^{N}(B_k - \bar{B})^2}, \tag{34}$$

when $N \to \infty$, $\hat{\sigma}_{\bar{B}} \to 0$ and $\bar{B} = E(B)$, while $\hat{\sigma}_B \to$ constant.

We may naturally raise the question: how can we determine N to fulfill our precision of $\bar{B} \to E(B)$? From sampling theory, if a single sample gives the precision $\hat{\sigma}_1$, then K groups of total N samples give the precision:

$$\hat{\sigma}_N = \frac{\hat{\sigma}_1}{\sqrt{N}} = \frac{\hat{\sigma}_1}{\sqrt{kK}} = \frac{\hat{\sigma}_k}{\sqrt{K}} \tag{35}$$

So if we have sampled a group with k replications and get a precision of $\hat{\sigma}_k$, and we are asking a precision of, say, $\hat{\sigma} \le 0.1\bar{B}$, the K (and so for $N = kK$) value can be estimated by

$$\frac{\hat{\sigma}_k}{\sqrt{K}} = 0.1\bar{B},\ K = \left(\frac{\hat{\sigma}_k}{0.1\bar{B}}\right)^2. \tag{36}$$

Applying the above to our situation, we have only one OFAD trial R and we have made 120 bootstrap replications B.

v.iv. Variance as a function of position

The bootstrap method can also provide a method to estimate the variance $\hat{\sigma}_R$ of the parameter $\hat{\theta}$ over whole pickle.

1. To get the variance as a function of position, we generate 100 uniform grid points $\grave{x}$ within the pickle by using

$$x_i = \rho_{i'}\cos\theta_{j'};\ y_i = \rho_{i'}\sin\theta_{j'};\ i = 1{,}100,\ i' = 1, 5;\ j' = 1, 20. \quad (37)$$

2. Calculate residuals between the reference solution R and the kth bootstrap solution B_k (k=1,2,...,N) for the ith (i=1,100) grid point:

$$\grave{r}_{ik} = \Delta\grave{x}(\grave{x}_i;B_k) - \Delta\grave{x}(\grave{x}_i;R) \quad (38)$$

3. Summing over N bootstrap replications, we estimate the bias and the variance for the ith point:

$$\hat{Bias}_i = \frac{1}{N}\sum_{k=1}^{N} r_{ik} \quad (39)$$

$$\hat{\sigma}_{B_i} = \hat{Var}_i = \sqrt{\frac{1}{N}\sum_{k=1}^{N}(r_{ik} - \bar{r}_{ik})^2}. \quad (40)$$

4. Applying the bootstrap assumption: $\hat{\sigma}_{R_i} \approx \hat{\sigma}_{B_i}$, we obtain an estimate of the variance $\hat{\sigma}_R$ over all pickle points. The contour maps for the reduction variance from Eq. (40) over a uniform grid can tell us about which region is most suitable for astrometry. Figure 4 shows that the expected error introduced into a star position by the derived OFAD will be less than 2 mas over almost the entire FGS field of view.

v.v. Variance of estimated parameters

The formal variances that are calculated as part of the least squares estimation are too large due to large correlations between the parameters. This is a particular problem with the star positions in the OFAD analysis. Since the positions of all of the stars depend in the same SSE parameters and OFAD coefficients they are all highly correlated. Consequently, we have calculated the variances of the estimated star positions using the bootstrap method just described. These variances are given in Table 2. We have performed similar calculations for the SSE parameters and found

that the variances that are calculated by the standard least squares method and the bootstrap method agree quite well.

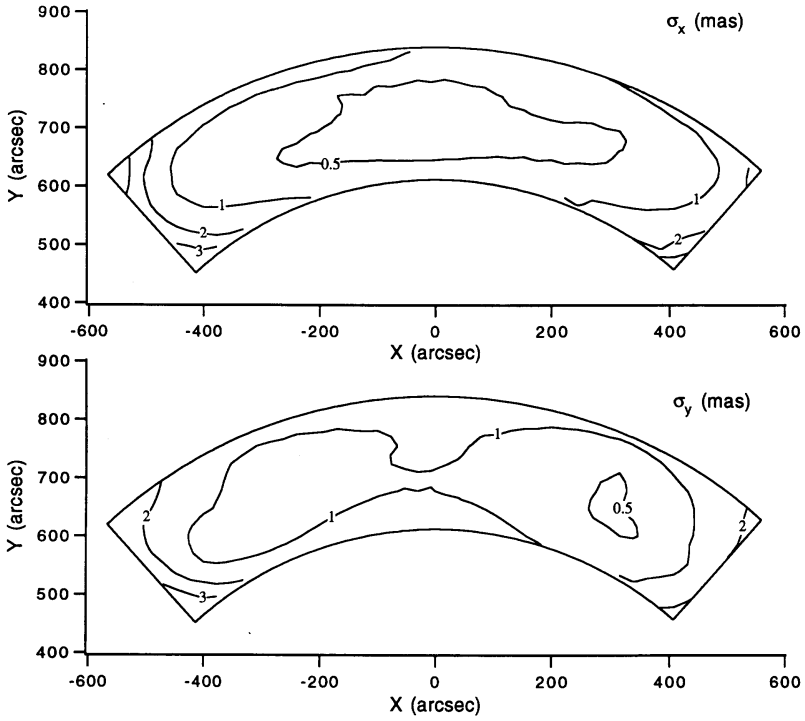

Figure 4: The expected error that will be introduced into a reduced FGS number 3 observation, due to the uncertainty in the OFAD polynomial, as calculated by a bootstrap analysis. Note that the root-sum-square contribution of the OFAD uncertainty is less than two milliarcseconds over almost the entire field of view.

VI. Remaining Work and Conclusions

As has already been stated, the data LTSTAB orbits were not included in the analysis described in this report. That analysis is on-going and an interim report is being released concurrently with this report.

Beyond the time dependence of the OFAD, the most significant unresolved issue concerning the OFAD is that of a possible lateral color effect. If there are significant lateral color effects in the FGS then they should be separately calibrated and the OFAD data re-analyzed to take these effects into account. In fact, a lateral color calibration was run on 23 December 1991. However, so much time elapsed between the execution of the lateral color and the OFAD calibrations that it has proven very difficult to connect the two calibrations. This analysis is still in progress.

The plate scale of the OTA/FGS system must be calibrated as well. This can be done in any of several different ways. Two methods that have been suggested are by use of stars that are part of the HIPPARCOS spacecraft catalog or by use of the motion of a minor planet. A calibration by the first method was begun in the spring of 1993 and

should yield a value for the plate scale that is accurate to a few milliseconds of arc over the FGS field of view.

Finally, the OFAD calibration that has been described here was made using the F583W filter. This filter is an essentially clear filter that has a pass band that is about 2340Å wide and is centered on 5830Å. FGS 3 has four other filters that can be used. They are a 2/3 pupil stop and red, yellow, and neutral density filters. Precise positional astrometry with any of these filters will require a cross filter calibration so that the OFAD measured with the clear filter can be used with the other filters.

The Astrometry Science Team is supported by NASA Grant No. NAG5-1603. The authors warmly acknowledge the interactions we have had, over many years, with Gary Welter, of Computer Sciences Corporation. Dr. Welter has done an immense amount of work on the operational calibration of the FGS and he has been an invaluable asset toward our scientific calibration. We are also grateful to J. Keith Kalinowski, of NASA/GSFC, for his many useful suggestions about the design and execution of the OFAD calibration observations.

References

Benedict, G.F. et al. 1992, PASP 194, 958

Bradley, A., Abramowicz-Reed, A., Story, D., Benedict, G. & Jefferys, W. 1991, PASP 103, 317

Burrows, C.J. et al. 1991, ApJ 369, L21

Cudworth, K.M. 1971, AJ 76, 475

Efron, B. 1982, The Jackknife, the Bootstrap and Other Resampling Plans, SIAM, Philadelphia

Fresneau, A. 1985, Hubble Space Telescope Fine Guidance Sensors Instrument Handbook, The Space Telescope Science Institute, Baltimore

Ftaclas, C. et al. 1993, Ap. Opt. 32, 1696

Jefferys, W.H. 1979, AJ 84, 1775

Jefferys, W.H. 1987, AJ 93, 755

Jefferys, W.H. 1990, Biometrika 77, 597

Jefferys, W.H., Fitzpatrick, M.J. & McArthur, B.E. 1988, Celest. Mech. 41, 39

Lasker, B.M., Jenkner, H. & Russell, J.L. 1988, in IAU Symp. No. 133, Mapping the Sky-Past Heritage and Future Directions, eds. S. Debarbat et al., Kluwer, Dordrecht, p. 229.

McNamara, B. and Sekiguchi, K. 1986, AJ 91, 557

Murray, C.A. 1983, Vectorial Astrometry, Adam Hilger, Bristol, p. 21

Wang, Q. 1990, Statistical Analysis of OFAD of *HST* using Bootstrap Method, M.A. Thesis, The University of Texas at Austin

TABLE 2. Estimated positions of the stars from 19 orbits of HST data taken for the OFAD calibration. The star numbers labeled MS# and CD# refer to the indices used by McNamara and Sekiguchi (1986) and Cudworth (1971), respectively. We have calculated absolute positions from the estimated relative positions ξ, η using $\alpha_o = 92.^{\circ}28890496$, $\delta_o = 24.^{\circ}58078484$, $\theta_o = 89.^{\circ}817036$. The V magnitudes were obtained from the *Hubble Space Telescope Guide Star Catalog* (Lasker, Jenkner, and Russell 1988) and are intended as an aid in identification only.

#	MS#	CD#	ξ	η	σ_ξ	σ_η	α (J2000)	δ	V
81			872.5462	791.9500	0.0027	0.0076	92.02207053	24.36133785	13.51
9			653.7647	786.2973	0.0015	0.0044	92.08878648	24.36281700	13.25
572			638.2968	850.2741	0.0023	0.0049	92.09346830	24.34503800	12.23
906			597.5594	680.1915	0.0019	0.0036	92.10598600	24.39226282	12.02
877			590.9608	652.0120	0.0014	0.0033	92.10801482	24.40008706	12.00
856			579.5590	538.8209	0.0030	0.0040	92.11155869	24.43152309	13.52
627			574.8319	912.4411	0.0018	0.0037	92.11278156	24.32773673	10.13
628			574.7750	937.5631	0.0031	0.0041	92.11278416	24.32075832	11.66
543			574.5118	889.8787	0.0024	0.0043	92.11289240	24.33400394	10.93
584			551.5653	974.9426	0.0032	0.0040	92.11983663	24.31036252	12.01
883			550.1506	630.4773	0.0020	0.0033	92.12047582	24.40604712	12.39
419			545.1814	845.7430	0.0017	0.0032	92.12186093	24.34624809	12.07
629			515.7988	782.6117	0.0019	0.0032	92.13085905	24.36376822	10.84
876			513.0989	344.4630	0.0033	0.0035	92.13195765	24.48547489	11.73
539			506.4927	811.7363	0.0014	0.0027	92.13367834	24.35567269	10.40
951			492.8937	476.1573	0.0030	0.0034	92.13804033	24.44888148	9.74
712			448.3656	856.8739	0.0016	0.0022	92.15137180	24.34310001	12.59
714	99	255	443.2047	791.5481	0.0013	0.0020	92.15298938	24.36124300	11.99
886			404.1424	463.1985	0.0023	0.0024	92.16513092	24.45242699	13.17
967	114	272	401.6386	649.8831	0.0010	0.0015	92.16576365	24.40056851	9.91
985	116	274	397.4187	744.4405	0.0010	0.0015	92.16698405	24.37429978	12.27
756	120	277	385.8561	803.5714	0.0012	0.0017	92.17046797	24.35786702	12.04
972			383.9666	500.8326	0.0021	0.0020	92.17126059	24.44196010	13.64
897	129	284	360.9692	634.3715	0.0018	0.0019	92.17818005	24.40485083	12.98
614	130	287	356.2041	946.7008	0.0019	0.0019	92.17940445	24.31808912	11.89
894	134	288	351.5530	580.3633	0.0010	0.0013	92.18109210	24.41984685	10.22
934			313.5950	393.3687	0.0026	0.0022	92.19281446	24.47176391	11.48
948	155	312	307.1579	667.5615	0.0008	0.0009	92.19456881	24.39559475	11.68
514	163	317	289.9747	824.8970	0.0011	0.0011	92.19968745	24.35187823	11.64
520	165	318	286.9921	964.1637	0.0028	0.0028	92.20048826	24.31319070	11.36
978	171	323	277.0894	560.8813	0.0012	0.0012	92.20382394	24.42520694	12.54
919	179	331	261.1165	530.6333	0.0014	0.0015	92.20872108	24.43359766	9.33
817	188	337	240.4090	807.7547	0.0012	0.0011	92.21481413	24.35660420	10.91
975	196	345	217.2856	708.7570	0.0006	0.0007	92.22194667	24.38408643	12.85
607	203	350	206.4610	763.7732	0.0008	0.0007	92.22520208	24.36879594	10.87
947	213	363	183.6265	643.8614	0.0007	0.0008	92.23226719	24.40208734	11.05
509	218	371	173.7209	797.3821	0.0008	0.0008	92.23515723	24.35943494	8.08
964	220	374	157.9684	667.1567	0.0008	0.0008	92.24007335	24.39559638	10.47
845	240	389	121.2729	637.6745	0.0008	0.0009	92.25129212	24.40375654	11.66
688	243	393	115.0819	778.7659	0.0017	0.0018	92.25305425	24.36455941	9.88
732	247	398	97.1370	744.8082	0.0006	0.0007	92.25855705	24.37397739	10.63
729	250		86.7727	778.7618	0.0014	0.0013	92.26168670	24.36453721	11.69
737	251		78.6382	797.0761	0.0008	0.0009	92.26415032	24.35944312	12.23
478	254	405	65.6711	777.2251	0.0009	0.0011	92.26812270	24.36494639	13.09
554			56.6148	852.6930	0.0011	0.0011	92.27081379	24.34397534	11.50
912			55.0977	696.4795	0.0006	0.0010	92.27142243	24.38736678	12.35
853	277	427	20.6260	739.8682	0.0005	0.0009	92.28189433	24.37528463	10.25
875	288	434	0.5456	694.3468	0.0016	0.0019	92.28806231	24.38791184	12.35
932	294	439	-8.7250	670.8286	0.0006	0.0010	92.29091275	24.39443644	11.15
868	297	443	-14.9165	686.2715	0.0010	0.0014	92.29278604	24.39014121	10.95
710	298	445	-21.3444	824.6293	0.0009	0.0012	92.29461003	24.35170265	13.26
946	315	458	-47.8180	564.5539	0.0030	0.0026	92.30294314	24.42392185	12.09
918	316	459	-48.5950	629.0164	0.0007	0.0012	92.30311537	24.40601490	10.00
674	338	486	-107.8883	873.5249	0.0014	0.0014	92.32094646	24.33804046	9.36
885	341	488	-107.6786	574.0248	0.0021	0.0024	92.32119534	24.42123515	13.27
496	350	500	-125.5687	764.3660	0.0008	0.0011	92.32645196	24.36834549	9.79
980	361	510	-153.3241	674.2172	0.0006	0.0010	92.33501269	24.39335986	11.05
631	364	513	-156.2286	760.9498	0.0006	0.0009	92.33580515	24.36926465	10.69
687	363	514	-157.0757	934.4278	0.0021	0.0028	92.33587665	24.32107537	10.85
962	369	515	-170.2168	518.5160	0.0023	0.0023	92.34033429	24.43659346	12.92
679	375	520	-185.3800	863.5363	0.0010	0.0012	92.34458229	24.34073948	11.43
963	386	529	-202.1027	562.2854	0.0013	0.0017	92.35001438	24.42440344	12.30
699	394	537	-221.5466	768.5136	0.0022	0.0023	92.35571507	24.36709816	12.53
983	396	539	-222.5051	628.9943	0.0008	0.0012	92.35616384	24.40585250	11.43
470	397	542	-227.2442	798.1468	0.0009	0.0009	92.35741919	24.35886086	12.29
957	401	547	-233.9595	719.9456	0.0007	0.0009	92.35955510	24.38057653	9.47
656	405	551	-246.3449	764.8312	0.0011	0.0012	92.36328125	24.36809551	11.66
590			-254.7560	975.3324	0.0025	0.0025	92.36560577	24.30961409	12.33
989	412		-273.2967	651.2125	0.0014	0.0016	92.37163129	24.39962806	13.35
913			-297.5941	596.5943	0.0010	0.0012	92.37910647	24.41477393	13.30
596	426	570	-306.3110	892.1581	0.0014	0.0016	92.38141761	24.33266363	11.46
935	428	571	-312.6481	681.4128	0.0008	0.0011	92.38359848	24.39119715	11.14
903			-329.8979	383.1516	0.0027	0.0026	92.38921601	24.47402845	11.44
480	433	579	-344.6161	912.8653	0.0018	0.0018	92.39307030	24.32687004	12.75
603	434	580	-345.4622	866.1558	0.0013	0.0012	92.39338439	24.33984399	10.63
862	449	598	-372.4204	576.6086	0.0009	0.0014	92.40195705	24.42024381	12.77
950	451	601	-378.3219	726.1392	0.0010	0.0013	92.40357401	24.37870106	11.19
489	454	603	-381.3933	805.0586	0.0011	0.0012	92.40441382	24.35677560	13.12
915	456	605	-391.6268	673.6241	0.0008	0.0011	92.40769643	24.39327362	13.48
719	457	606	-393.9079	919.1540	0.0023	0.0025	92.40808879	24.32506833	10.04
798			-406.7233	836.6876	0.0011	0.0012	92.41209795	24.34796119	12.22
900	468	619	-411.2715	535.2052	0.0010	0.0016	92.41386101	24.43170092	12.24
564	472	622	-429.6251	920.9994	0.0012	0.0015	92.41897443	24.32451506	11.73
859			-434.1128	407.8234	0.0029	0.0031	92.42099098	24.46705834	13.67
944			-464.7764	424.4672	0.0025	0.0025	92.43032751	24.46239945	13.05
659	481	633	-478.3271	739.3035	0.0014	0.0018	92.43405536	24.37492940	13.11
706	498	652	-545.9203	755.3201	0.0025	0.0027	92.45464705	24.37039920	13.75
797	502	656	-552.2129	793.5396	0.0017	0.0022	92.45651467	24.35977503	9.91
445	506	663	-605.0441	997.6470	0.0030	0.0038	92.47234325	24.30301297	13.57
457	507	664	-607.4605	740.4768	0.0012	0.0024	92.47343407	24.37444603	10.63
965			-888.9762	717.0597	0.0023	0.0063	92.55932109	24.38057188	13.18

Maintaining the FGS3 OFAD Calibration with the Long-Term Stability Test

A. Whipple[1], W. Jefferys[1], Q. Wang[1], B. McArthur[1], G. F. Benedict[1], E. Nelan[1]
D. Story[1] and L. Abramowicz-Reed[2]

Abstract

The Hubble Space Telescope carries three Fine Guidance Sensors (FGS) that serve as part of the Pointing Control System and can be used for millisecond of arc astrometry on stars as faint as V=17. The *HST* Ritchey-Chrétien design produces optical distortions in the field of view of the telescope, which because of residual misalignments, must be calibrated on-orbit for any instrument. The series of optical field angle distortion (OFAD) calibrations begun in December 1990 has shown evidence that some aspects of the OFAD change with time. A series of long-term stability (LTSTAB) tests was begun on 2 December 1992 to characterize and monitor these changes. Each LTSTAB test consists of a single orbit visit to the ecliptic open cluster M35 which was used for the OFAD. As of the writing of this report (November 1993) eight LTSTAB tests have been performed. The current status of our analysis of these data is summarized in this report.

I. Introduction

The *HST* is a Cassegrain telescope of the Ritchey-Chrétien design. The prescription of the Optical Telescope Assembly (OTA) contains optical field angle distortion (OFAD) and some astigmatism. This report is intended as one of a series of appendices to the final report on the Optical Field Angle Distortion (OFAD) Calibration (Jefferys et al., this volume). A familiarity with that report is assumed in the following.

For reasons that are not well understood at this time, the metrology of the FGS optical system, and hence the OFAD, has not fully stabilized. A post-launch period of change was expected since many of the structures in the FGS are made of graphite epoxy which shrinks in a non-uniform way due to water desorption. While the amount of change that is observed has decreased since the first few months after launch, there remains a time varying part of the distortions that are observed by the FGS. We have had to generalize our OFAD model and our calibration tests to account for these time dependent changes. A series of long-term stability (LTSTAB) tests was begun on 2 December 1992 to characterize and monitor these changes. Each LTSTAB test consists of a single orbit visit to the ecliptic open cluster M35 which was used for the OFAD calibration. As of the date of this report, eight LTSTAB tests have been

1. Astronomy Department and McDonald Observatory, University of Texas, Austin, Texas 78712
2. Hughes Danbury Optical Systems, Danbury, Connecticut 06810

performed. The current status of our analysis of these data is summarized in this report.

II. The LTSTAB Model

Our present model of the distortion changes reflects the simplest physically possible change within the FGS unit. We use the qualifier of "physically possible" to exclude changes such as the magnification of the *HST* OTA. The magnification of the telescope could not change enough to model the observed changes in the FGS distortions without this change being readily observable in the *HST* camera images. Such a change has not been observed by the cameras and so we have excluded this possibility from our modeling.

The simplest physically possible change within the FGS unit would be a change in only the relative positions of the two flat mirrors that make up star selector A. A change in the relative positions of these two mirrors would cause a change in the magnitude of the star selector encoder parameter ρ_A. The star selector encoder parameters ρ_A, ρ_B, k_A, k_B, and M are the instrumental parameters that relate the observed rotation angles θ_A and θ_B to the Cartesian coordinates x and y via the equations

$$\begin{aligned}
\cos\rho &= \cos\rho_A\cos\rho_B + \sin\rho_A\sin\rho_B\cos(180^\circ - q) \\
\sin\rho\sin p &= \sin\rho_B\sin(180^\circ - q) \\
\sin\rho\cos p &= \cos\rho_B\sin\rho_A - \sin\rho_B\cos\rho_A\cos(180^\circ - q)
\end{aligned} \tag{1}$$

with $q = (\theta_B + k_B) - (\theta_A + k_A)$ and $p = \phi - \theta_A - k_A$ and

$$\begin{aligned}
x &= \sin\frac{\rho}{M}\cos\phi \\
y &= \sin\frac{\rho}{M}\sin\phi
\end{aligned} \tag{2}$$

Figure 2 in Jefferys et al. (1993) shows the geometry of the FGS coordinates. For completeness, we give the functional form of the OFAD model used in our analysis:

$$\begin{aligned}
\Delta x_{dist}(x, y; a_{ij}) = x_{true} - x = {} & a_{00} + a_{10}x + a_{01}y + a_{20}x^2 + a_{11}xy + a_{30}x(x^2 + y^2) \\
& + a_{21}x(x^2 - y^2) + a_{12}y(y^2 - x^2) + a_{03}y(y^2 + x^2) \\
& + a_{50}x(x^2 + y^2)^2 + a_{41}y(y^2 + x^2)^2 + a_{32}x(x^4 - y^4) \\
& + a_{23}y(y^4 - x^4) + a_{14}x(x^2 - y^2)^2 + a_{05}y(y^2 - x^2)^2
\end{aligned} \tag{3}$$

$$\Delta y_{dist}(x, y; b_{ij}) = y_{true} - y = b_{00} + b_{10}x + b_{01}y + b_{20}x^2 + b_{11}xy + b_{30}x(x^2 + y^2) + b_{21}x(x^2 - y^2) + b_{12}y(y^2 - x^2) + b_{03}y(y^2 + x^2) + b_{50}x(x^2 + y^2)^2 + b_{41}y(y^2 + x^2)^2 + b_{32}x(x^4 - y^4) + b_{23}y(y^4 - x^4) + b_{14}x(x^2 - y^2)^2 + b_{05}y(y^2 - x^2)^2$$

where the coefficients a_{ij}, b_{ij} are the constants that are estimated.

III. The HST Observations

The long-term stability test (LTSTAB for short) program consists of periodic visits (ideally once per month) to the M35 field used for the OFAD. In fact, M35 was chosen for the OFAD calibration because of the need to run the LTSTAB tests. Since M35 is in the ecliptic, the telescope does not gradually roll about this field throughout the year as it does for a target off the ecliptic. Instead, the telescope "flips" 180° when M35 gets closest to the anti-solar point (to be precise, the telescope rolls 180° between December 20 and December 28 with the bulk of the roll occurring on December 24). This means that we can observe the calibration field at two fixed orientations; one in the fall and one in the spring. This maximizes our sensitivity to real changes in the OFAD and minimizes our sensitivity to uncertainties in the OFAD that might appear as changes if the telescope gradually rolled through the calibration field. Each spring the LTSTAB test consists of a single orbit of observations that repeat the central pointing of the OFAD. The fall LTSTAB tests also consist of a single orbit of observations but are rolled approximately 180° about the central pointing of the OFAD calibration. These two pointings are highlighted by the heavy lines in Figure 1 in Jefferys et al., this volume. Two executions of the LTSTAB test were made before the OFAD calibration; on December 2 and 14, and four were run after the OFAD calibration; on April 5, 18, and 19 and on August 26. We expect to continue the LTSTAB tests, at a rate of approximately once per month, whenever M35 is observable.

IV. Results from Our Analysis of the LTSTAB Data

We have subjected the data from the eight orbits from the LTSTAB test runs to a least-squares estimation. The star positions, the OFAD coefficients, a_{ij} and b_{ij}, and the star selector parameters, ρ_B, k_A, k_B, and M were all held fixed to the values determined from the 19 uncorrupted orbits obtained during the 10 January 1993 OFAD calibration. These star positions and parameters are given in Tables 1 and 2 of Jefferys et al. (1993). A unit pointing quaternion, two linear drift parameters, and ρ_A were estimated for each LTSTAB orbit.

Since the *HST* observations are relatively insensitive to absolute scale, the variances of all scale-like quantities in an OFAD solution are inherently large. But when the other parameters are held fixed and only ρ_A is estimated, the estimated variances are approximately equal to the variance of the factional change in ρ_A,

$$\Delta\rho_{A_i} = \frac{(\rho_{A_i} - \rho_{A_{OFAD}})}{\rho_{A_{OFAD}}}. \quad (4)$$

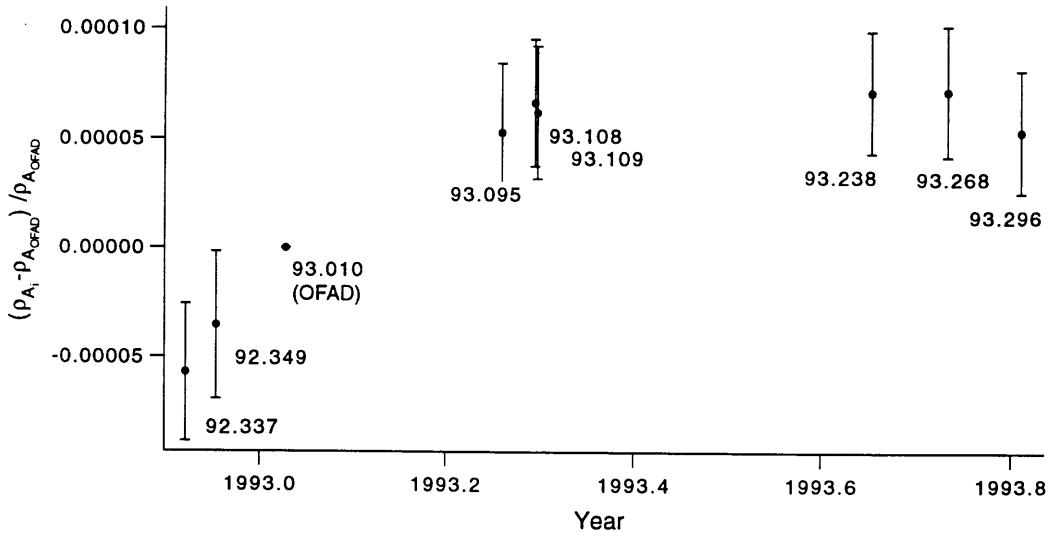

Fig. 1. The change in the star selector servo assembly angle ρ_A as deduced from the eight LTSTAB tests. The increase in ρ_A is equivalent to an apparent contraction of a star field.

The time evolution of the SSE parameter ρ_A, with the calculated variances, is shown in Figure 1. It is obvious that statistically significant changes in ρ_A are occurring that will require continued monitoring. The effect of this change is analogous to what would happen if one were to stretch a ruler. The spacing between the marks would get larger and measured distances would get smaller. In a similar fashion, as ρ_A increases, the measured separations between stars decreases. In terms of plate constants, this means that $a^2 + b^2 > 1$ in the equations

$$a\xi + b\eta + c = x \quad (5)$$

$$-b\xi + a\eta + d = y$$

when a plate from time t is overlaid on a plate from time t_0 where $t > t_0$. This is consistent with the changes observed in long- and short-term astrometric stability tests as summarized in Benedict et al. (this volume). The LTSTAB data have not revealed that higher order changes in the OFAD are occurring. The statistics of the residuals from the fits to the eight LTSTAB orbits are summarized in Table 1. For comparison, the RMS of the residuals from the 548 individual observations from the 19 OFAD orbits were 2.3 mas along both the x and y axes.

TABLE 1. Statistics of the residuals from the first eight executions of the FGS 3 LTSTAB test.

			RMS (mas)			
Date	Orientation	# obs	x	y	# GS	Dejittered
1992.337	fall	24	4.2	3.1	2	yes
1992.349	fall	22	3.1	3.2	2	yes
1993.095	spring	29	2.5	2.9	1	no
1993.108	spring	29	3.3	3.1	1	no
1993.109	spring	29	2.5	3.5	1	no
1993.238	fall	27	2.9	5.0	1	no
1993.268	fall	26	3.1	4.5	1	no
1993.296	fall	26	3.4	4.6	1	no
Total			3.2	3.8		

V. Remaining Work and Conclusions

The LTSTAB orbits contain much information about constant quantities as well as time-dependent parameters. In particular, the positions of the stars change very slowly, if at all, and it is hoped that the coefficients of the OFAD polynomial do not change. Moreover, the fall orientation LTSTAB tests have the potential to make a significant contribution to the determination of the OFAD coefficients because of their 180° roll relative to the spring pointing. Consequently, we are working on a "grand-OFAD" solution that will simultaneously use all of the OFAD plus LTSTAB orbits to determine the constant and time-dependent parts of the FGS distortion model.

As more LTSTAB tests are run, especially at approximately one month intervals, we will be able to finally determine whether or not changes are occurring in higher order terms of the distortion model. We will also be able to determine an appropriate functional form for the time-dependent parameters and estimate the relevant coefficients. This will permit optimal interpolation of the distortion model to any epoch. Looking forward, the continued execution of the LTSTAB tests is mandatory to maintain the OFAD calibration which, in turn, is essential for all future astrometry science with *HST*.

Astrometric Stability and Precision of Fine Guidance Sensor #3: The Parallax and Proper Motion of Proxima Centauri

G. F. Benedict[1], B. McArthur[1], E. Nelan[1], D. Story[1], A. L. Whipple[1], W. H. Jefferys[2]
Q. Wang[2], P. J. Shelus[1], P. D. Hemenway[1], J. McCartney[1], Wm. F. van Altena[3]
R. Duncombe[4], O. G. Franz[5] and L. W. Fredrick[6]

Abstract

Demonstrating the utility of *HST* for astrometry, we obtain $\pi = 0.7692 \pm 0.0004$ arcsec and $\mu = 3.8531 \pm 0.0005$ arcsec per year, for Proxima Centauri. Achieving this precision required 42 observation sets spaced over 1.5 years. Parallaxes with precision slightly better than 0.001 arcsec can be obtained with 11 observations spanning one year.

I. Observations

We present a progress report on astrometry of Proxima Centauri with the *HST* FGS 3. Proxima Cen (α Cen C; V645 Cen) is a known flare star. The spectral type is M5Ve and $M_V = 15.45$, V = 11.22 (Walker 1981). The mass of Proxima Cen is estimated to be $0.11 M_{Sun}$ (Kirkpatrick and McCarthy, 1993). An early assessment of astrometry with FGS 3 can be found in Benedict et al. (1992). Benedict et al. (1993) presents a more detailed discussion of the astrometry of the reference stars. The scientific motivation for these observations is the determination of an upper limit for non-stellar companions to Proxima Cen. Since our monitoring is incomplete, we will discuss the planet search at a later time.

Our astrometric results thus far are based on 42 observation sets (orbits) acquired between 23 March 1992 to 5 October 1993. Figure 1 shows the field containing Proxima Cen and the reference stars. We attempted 49 data sets. Six were lost or fatally corrupted due to jitter and/or loss of lock. One GTO set was lost to safe-mode. We have experienced no losses of lock since January 1993, after a significant modification to the Pointing Control System software. We suffered one GS Acquisition failure. Since this is a monitoring project, we would prefer no gaps in coverage. We have experienced several. One is natural, due to the *HST* sun constraint. A second gap occurred due to FGS 2 bearing difficulties.

1. McDonald Observatory, University of Texas, Austin, TX 78712
2. Astronomy Department, University of Texas, Austin, TX 78712
3. Yale University, New Haven, CT 06511
4. Aerospace Engineering Department, University of Texas, Austin, TX 78712
5. Lowell Observatory, Flagstaff, AZ 86001
6. University of Virginia, Charlottesville, VA 22903

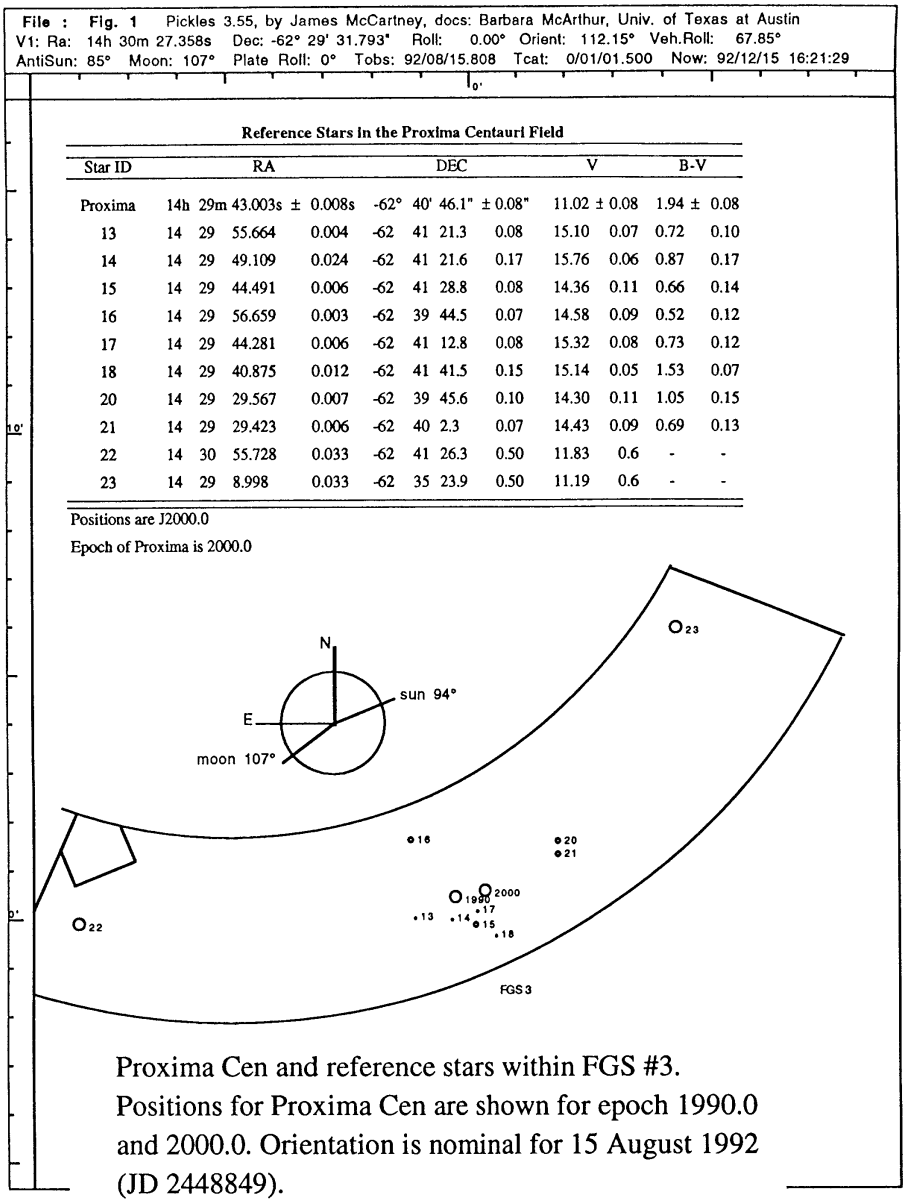

Proxima Cen and reference stars within FGS #3. Positions for Proxima Cen are shown for epoch 1990.0 and 2000.0. Orientation is nominal for 15 August 1992 (JD 2448849).

Figure 1

What have we done to pre-process these data?

- median filtered to reduce jitter
- secondary mirror breathing treated as linear drift
- known encoder bit-error pattern (LSB) included
- asphere and pick-off corrections included
- our best Optical Field Angle Distortion mapping (Jefferys et al., this volume)

These interim results do not include corrections for field dependent k-factors, de-jittering, and possible color effects. Hence, there is room for improvement.

II. The Astrometric Model, Resulting Precision, and Scale Stability

Every astrometry observation is an act of calibration. With our 42 observation sets (with 5 - 7 reference stars per set) we solve for

- plate (set) constants: a, b, c, d, e, f
- star parameters: proper motion, μ; and parallax, π
- R, roll orientation of the constraint plate with respect to RA and DEC

in the system of equations:

$$\xi = aX + bY + c - \mu_x t - (p_x \times \cos(R) - p_y \times \sin(R))\,\pi$$

$$\eta = dX + eY + f - \mu_y t - (p_x \times \sin(R) + p_y \times \cos(R))$$

where the X, Y are positions of the stars in each data set, p_x and p_y are parallax factors. The ξ and η are x, y positions for the plate (observation set) chosen as our constraint, 1992, day 135.

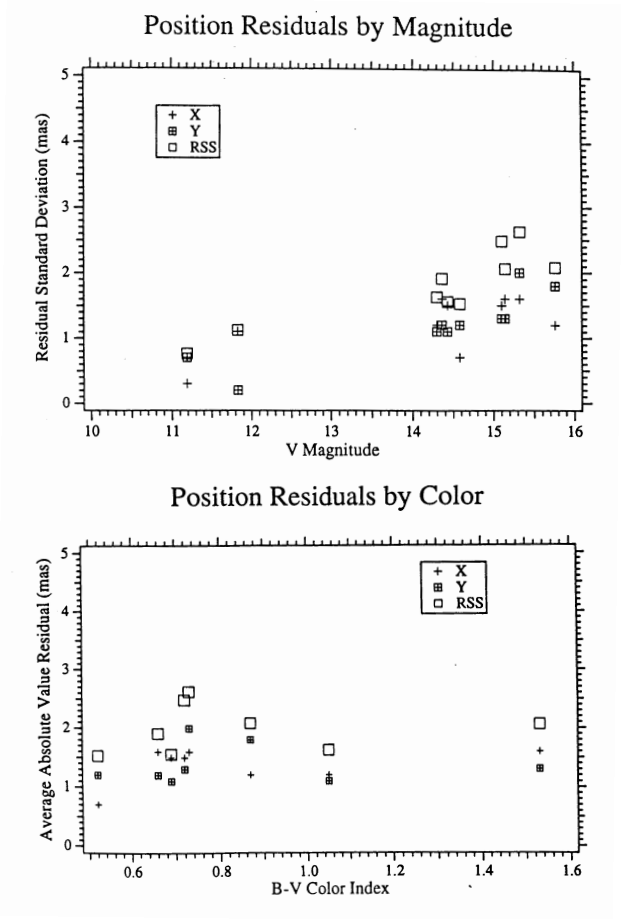

Figure 2

From Figure 1 we see that the average magnitude of our reference frame is V~15. Hence, parallax and galactic rotation effects would be at a level of ~0.5 millisecond of arc per year level (van Altena, 1993). Nonetheless, one reference star (18) is found to have a parallax π = 0.0031±0.0005 arcsec. After 3σ rejection, reference frame RSS average absolute value residual is 2.0 mas. The 3σ rejection resulted in 6 percent of the reference stars being rejected. Figure 2 shows the run of residual against star ID and against star color. Note that there are no statistically significant color terms for $0.52 < B - V < 1.53$.

We next explore the scale stability of the Proxima Cen reference frame by defining a global scale:

$$S = (ae - bd)^{1/2}$$

Figure 3 plots these values against time. We see significant variations. However, these variations are not typical scale variations due to primary-secondary mirror despace changes. They are most likely due to optical component shifts internal to FGS 3. See Whipple et al. in this volume for a discussion. The quality of the scale-like change is more important to *HST* FGS Astrometry than the quantity of the change. The gradual scale-like changes seen will be monitored, eventually understood, and removed. For now, the changes are absorbed into the astrometry coefficients. Lastly, note (Figure 3) that our totally independent long-term stability (LTSTAB) field shows quantitative agreement (Whipple et al., this volume).

III. Astrometric Results

The following table compares our interim Proxima Cen parallax and proper motion with a long-duration ground-based campaign. Errors are internal.

	HST	Ground
Study duration	1.5y	45y
# plates	41	130
Ref. stars <V>	14.9	12.3
Parallax	0.7692 ± 0.0004	0.773 ± 0.004 arcsec
Proper Motion	3.8531 ± 0.0005	3.8473 ± 0.0008 arcsec/year

The ground-based study is described in Kamper and Wesselink (1978). We can expect differences in proper motion due to motions in the reference frame. Ours, being fainter, has less motion and likely yields a more accurate proper motion for Proxima Cen. In a ground-based redetermination of the proper motion including more recent plate material van Altena & Yang (1992) get 3.8527 arcsec/year for the proper motion. Reference star 18 is included in the solution with its parallax.

We next discuss astrometry with a realistic set of observations. What does a one year campaign yield? We analyze an 11 observation set sub-set of the Proxima Cen data, representing one observation per month and find π = 0.7699±0.0007 arcsec and

μ = 3.8561±0.0013 arcsec/year. Modern ground-based CCD astrometry yields 0.001 arcsec precision parallaxes and 0.0006 arcsec/year precision proper motions for 3-5 year baselines (Monet et al. 1992). If you are in a hurry, use *HST*.

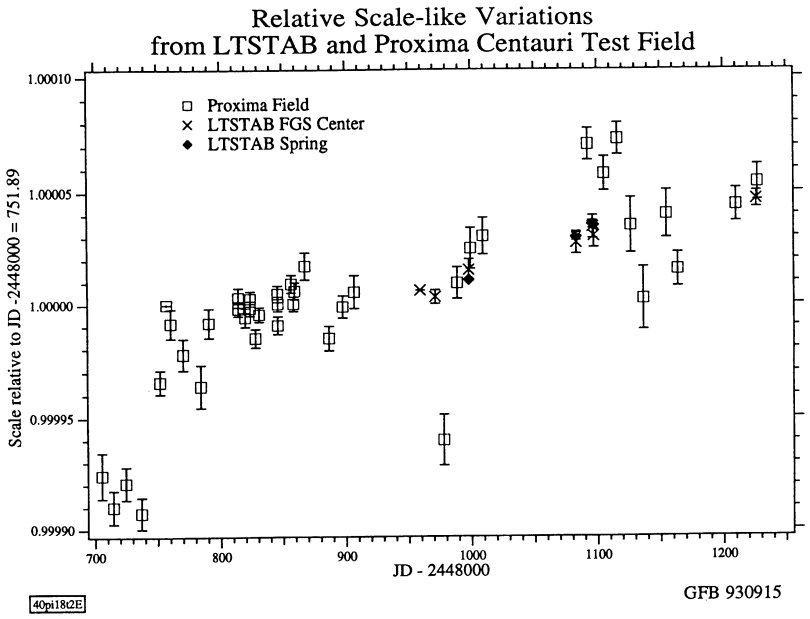

Figure 3

Conclusions

- We obtain astrometric precision of 0.0020 arcsec RSS per observation in the pickle center, better than pre-launch estimates.
- Scale-like variations seen in the Proxima Cen astrometry do not adversely affect our astrometry. The variations agree with the LTSTAB monitoring results (Whipple et al., this volume).
- A 1.5 year campaign with *HST* produces a parallax precise to 0.0004 arcsec, and agrees with a 45 year ground-based effort.
- Two parallax determinations from a single field with *HST* have precisions similar to the best ground-based techniques, but required one quarter the time.

References

Benedict, G. F. et al. 1992, PASP, 104, 958
Benedict, G. F. et al. 1993, submitted to PASP
Kamper, K. W. and Wesselink, A. J. 1978, AJ, 83, 1653
Kirkpatrick, D. and McCarthy, D. 1993. AJ in press
Monet, D. G. et al. 1992 AJ, 103, 638
van Altena, W. & Yang, T. 1992 private communication
van Altena, W. 1993 private communication
Walker, A. R. 1981, MNRAS, 195, 1029

Binary Star Astrometry and Photometry from Transfer-Function Scans with *HST* FGS3: Calibration, Stability, Precision, and Accuracy

O. G. Franz[1], J. N. Kreidl[1], L. H. Wasserman[1], A. J. Bradley[2], G. F. Benedict[3]
R. L. Duncombe[3], P. D. Hemenway[3], W. H. Jefferys[3], B. McArthur[3], J. E. McCartney[3]
E. Nelan[3], P. J. Shelus[3], D. Story[3], A. L. Whipple[3], L. W. Fredrick[4]
Wm. F. van Altena[5], M. G. Lattanzi[6] and L. G. Taff [6]

Abstract

We illustrate the concept of binary-star astrometry and photometry based upon observations with the Hubble Space Telescope Fine Guidance Sensors (FGS) in the Transfer Function (TF) Scan mode. Using data obtained over an 18-month interval in 1992-1993, we assess temporal TF stability and examine its significance for binary-star investigations by FGS transfer-function analysis. We present astrometric results for Cycle-2 scale-calibration binaries observed with FGS3. Analysis of multiple observations indicates a precision of 1 mas. We compare the measured relative component-positions with ephemeris values from orbits based upon extensive series of speckle observations. This comparison shows that the accuracy of binary-star astrometry with FGS3 in the TF-Scan mode is 1 mas.

I. Concept of Binary-Star Measurement by *HST* FGS Transfer Function Analysis

We assume the Transfer Function (TF) of a resolved binary star to be a linear superposition of two single-star functions. If $F(X)$ is the TF of a single star on the FGS X-axis, a double star will thus yield a TF of the form,

$$D(X) = A \times F(X + Z) + B \times F(X + Z + S)$$

where, A and B are the fractional intensities of the binary components, Z is a zero point offset, and S is the component-separation along the FGS X-axis. An equivalent expression exists in FGS-Y.

This concept is illustrated in Fig. 1 with data for ADS 11300 (= Hu 581 = WDS 18229+1458 (2000)), a visual binary of magnitude 8.3 and angular separation near 0.1 arcsec.

---

1. Lowell Observatory, Flagstaff, AZ 86001
2. Allied-Signal Aerospace Company
3. University of Texas at Austin, Austin, TX 78712
4. University of Virginia, Charlottesville, VA 22903
5. Yale University, New Haven, CT 06511
6. Space Telescope Science Institute, Baltimore, MD 21218

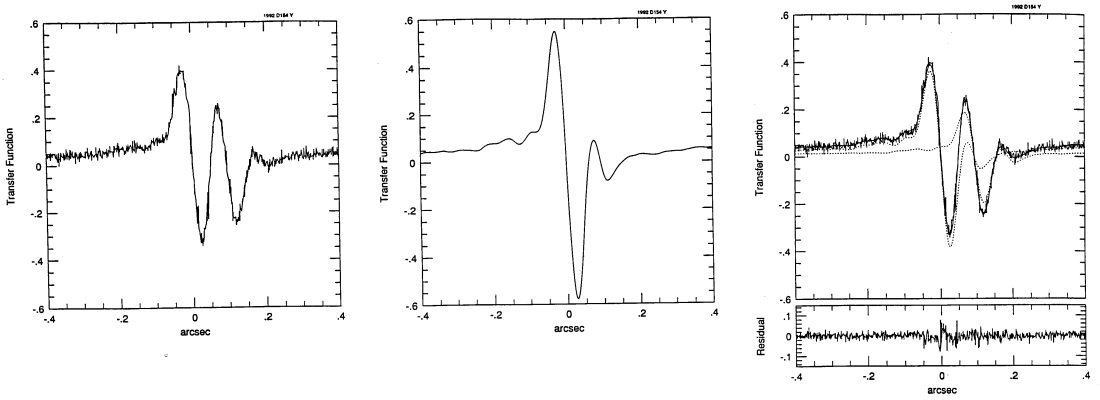

Figure 1: A sample Transfer Function (TF) of ADS 11300 (left) obtained on 1992 day 154 shows the binary well resolved on the FGS Y-axis. A smoothed single-star TF (middle) derived by co-addition of several de-jittered scans is used in the binary-star data analysis. The result of the analysis (right) is illustrated by a computed curve (smooth solid line) representing the best-fitting linear superposition of two single-star TFs (dotted lines). Residuals show no systematic differences between observed and computed binary-star TF.

II. Transfer Function Stability

Because analysis of binary-star scans obtained with the FGS requires accurate knowledge of the single-star Transfer Function (TF), it would be best to obtain such calibration data contemporaneously with every binary-star observation. However, this approach is not only costly in observing time, but also vulnerable to observational failures. It is thus important to examine the temporal TF-stability and to determine whether archival single-star data can be used without degradation of binary-star photometry and astrometry.

To assess temporal TF-stability and its significance for binary-star investigations, we have used single-star (Upgren 69) data from six separate dates over an 18-month interval in 1992-1993 to analyze TFs of ADS 11300 obtained on 1993 day 92. All scans were made near the center of the field of view (FOV) of FGS3. The values so derived for the angular separations of the binary components in X, Y, and for the magnitude difference are presented in Table I.

Table 1: Astrometric and Photometric Results for ADS 11300 from Observations of 1993 day 92 Analyzed with the Use of Single-Star Data, Both Contemporaneous and from Different Dates

single-star date		angular separation (arcsec)		mag. diff.
(year)	(day)	X	Y	
1992	049	–0.093	0.054	0.68
	098	–0.093	0.055	0.68
	154	–0.093	0.054	0.66
	245	–0.093	0.055	0.67
1993	*092*	*–0.093*	*0.054*	*0.69*
	217	–0.092	0.055	0.65

The small scatter of the tabulated values of angular separations and magnitude difference indicates remarkable stability of the single-star TFs from the six widely separated dates. It must be noted, however, that susceptibility of the analysis to effects of Transfer Function variations will grow with decreasing angular separation and increasing magnitude difference of the binary components.

III. Scale Calibration: Astrometric Precision and Accuracy

Binaries for scale calibration in the Transfer Function (TF) Scan mode were selected from a set of potential FGS calibration targets frequently observed by speckle interferometry with 4-m class telescopes. The plan was to derive, on the basis of well calibrated speckle measures, binary-star orbits that could yield, for any date of *HST*-FGS observation, accurate angular separations of the binary components.

In Table 2 we present, for two calibration binaries, angular separations determined from multiple sets of TF scans with FGS3. These scans, made near the center of the field of view, were reduced with the nominal, pre-launch scale value. Also given in Table 2 are the corresponding values of the angular separations derived from binary orbits based on speckle data.

Table 2: Scale Calibration — Preliminary Results

Binary Name	Date Observed	FGS Filter	Angular Separation (arcsec)	
			FGS3 TF Scans	Speckle Orbit
ADS 10360	93: 104	F5ND	0.121	0.120
		F5ND	0.120	
KUI 83	93: 148	F583W	0.323	0.322
		PUPIL	0.323	

Conclusions

Examination of the angular separation values listed in Table 2 for two calibration binaries leads to the following conclusions:

- Scale calibration observations of close binary stars with FGS3 in the Transfer Function (TF) Scan mode and near the center of the field of view (FOV) have shown that *for purposes of close binary-star astrometry, the present on-orbit scale is the same as the nominal pre-launch scale.*
- The astrometric *precision* for close binary stars observed with FGS 3 in the TF-Scan mode and near the center of the FOV is 1 millisecond of arc.
- The astrometric *accuracy* for close binary stars observed with FGS3 in the TF-Scan mode and near the center of the FOV is 1 millisecond of arc.

Centroiding Planetary Camera Stellar Images

T. M. Girard[1], W. F. van Altena[1], W. H. Jefferys[2], G. F. Benedict[2], P. D. Hemenway[2]
P. J. Shelus[2], O. G. Franz[3], L. W. Frederick[4], E. Nelan[2], D. Story[2], A. L. Whipple[2]
B. McArthur[2], L. Wasserman[3], J. McCartney[2], R. L. Duncombe[5]
J. M. Nunez[6] and A. Prades[6]

Abstract

The Space Telescope Astrometry Team is investigating the astrometric capabilities of the Planetary Camera. Our primary motivation for establishing an astrometric calibration of the PC is a long-term proper-motion study, the goal of which is to determine the internal velocity distributions of several globular clusters. The ultimate astrometric accuracy of the PC will be determined by 1) the accuracy to which the aberrated images can be "centered", and 2) the accuracy to which the distortions across the PC field can be modeled. Here we address the first issue and summarize our progress including results from a study of the use of maximum likelihood image reconstruction to improve the image center determinations. We are investigating the benefits to be gained by performing the image restoration on a grid which is finer than the actual PC pixel size by using subsampled synthetic PSFs from Tiny Tim and replicating a PC exposure of the globular cluster NGC 6752 for test purposes.

I. Motivation

Even with its aberrated images, the *HST* Planetary Camera allows imaging of individual main-sequence stars very near the cores of globular clusters. It is our goal to use the *HST* PC as an astrometric instrument to determine stellar proper motions within six globular clusters. The proper motions would yield:

- internal velocity dispersions for these six clusters,
- virial mass estimates for these clusters,
- kinematic distance estimates (statistical parallax),

1. Yale University, Astronomy Dept., P.O. Box 6666, New Haven, CT 06511
2. Astronomy Department and McDonald Observatory, University of Texas, Austin, TX 78712
3. Lowell Observatory, Flagstaff, AZ 86001
4. University of Virginia, Charlottesville, VA 22903-0818
5. University of Texas at Austin, Department of Aerospace Engineering, Austin, TX 78712
6. University of Barcelona, Spain

- and, for a subgroup of the more nearby clusters –

  (i) the radial and azimuthal velocity dispersions as a function of distance from the cluster center, and
  (ii) the degree to which energy equipartition exists between various stellar mass groups within the clusters

Instrument: Planetary Camera = 4 x 800 x 800 CCD, Scale = 0.043 arcsec/pixel

Desired astrometric accuracy:

- positions to ± 1 mas, (1/40 pixel)
- second epoch exposures after 5 years ⇒
- proper motions to ± 0.2 mas/yr (~5 km/s for d = 5 kpc) ⇒
- σ_v to ~ ± 1 km/s for d = 5 kpc
- Note: σ_v ~ 6 to 10 km/s for globular clusters)

III. Non-Reconstructed Images

Previous tests, (Girard and van Altena, 1990), using synthetic PC frames and a limited number of early-observation frames of the R136 region showed that 2 mas positional accuracy could be achieved for well-exposed images using Gaussian fitting of the raw intensity profiles. The accuracy quickly fell off for fainter images and in crowded regions.

Although we are interested in an application involving crowded fields with low signal-to-noise images, (the globular cluster program), it is worth noting the centering precision we have recently achieved with a set of high signal-to-noise, isolated PC stellar images. This series of PC frames, taken in conjunction with FGS observations intended to monitor the long-term stability of the FGS instrument frame, was taken with the same pointing on consecutive orbits. The PC fields contain from two to three well-exposed stars. We have fit the raw intensity profiles of the stars with our 2-D Gaussian centroider and estimated the centering precision from the deviations in the separation of star pairs. Based on 22 separation measures, the single-coordinate centroiding precision is 0.6 mas, (0.014 pixels)!

It must be stressed that this high level of repeatability is thus far demonstrated only over consecutive *HST* orbits and with nearly identical pointing, (the individual star positions varied by ~ 0.06 to 0.20 pixels).

IV. Reconstructed Images

Two PC frames of the globular cluster NGC 6752, (a 40-sec and 500-sec exposure with F675W), were used to test if image reconstruction could improve the positional accuracy. Approximately 55 (uncrowded) stars from PC-5 were used. The entire 800x800 pixel frame was restored using a maximum likelihood image reconstruction

code, (Nez and Llacer, 1990). Reconstructions were based on a synthetic PSF, generated by the Tiny Tim software package, and were halted after 100 iterations. The reconstructed intensity profiles were centered using the two-dimensional, Gaussian fitting routine. The long exposure positions were transformed into those of the short exposure to determine the unit weight measuring error. The results are presented in Table 1.

Table 1: Long-to-short exposure reduction results

	unit weight error (mas)			
	x	y	No. stars	Mag range
raw[a]	1.4	2.1	33[b]	2.3
PSF @ (200,600)	1.4	1.2	39	2.9
PSF @ (400, 400)	1.3	1.0	38	2.8
PSF @ (600,200)	0.8	0.8	42	3.3

a. This solution required the removal of many "outliers" both bright and faint, thus the unit weight errors may be underestimated in this solution.
b. The original target list consisted of 55 stars. Several of these were so saturated they did not center in any reductions. In addition, 8 to 10 very bright stars were eliminated due to a non-linear magnitude effect present.

These results suggest that 1 mas positional accuracy may be obtained with image reconstruction, for an uncrowded field of relatively well-exposed images. We do not consider these results conclusive, however. There are indications that the image positions were biased toward the center of the brightest pixel of each image, (i.e. the fractional pixel coordinates were not evenly distributed from 0.0 to 1.0). If this is the case, the effect would appear in both the long and short exposure reconstructions and the error estimates based on the above reductions would be invalidated.

V. Subsampled Reconstructions

Synthetic PSFs may be generated on arbitrarily fine grids, allowing the reconstruction to be performed on a grid spacing smaller than that of the detector, one that better samples the PSF. A subsampled reconstruction should be much less affected by the centering bias discussed above. We have used subsampled reconstructions, at subsampling factors of 1 through 5, to explore its effect on the final centered positions.

Two additional PC exposures of NGC 6752 have been used for this part of our study – the first, a 100 sec, F555W exposure; the second, a 100 sec, F785LP exposure. A 128 x 128 subframe containing roughly 40 faint stellar images was extracted from PC 5. Tiny Tim PSFs were calculated, in both filters, at the center of the subframe, and for each subsampling factor from 1 to 5. The subframes were then processed through 80 iterations of the reconstruction code.

Twenty-five stars successfully centered on each of the 1x processed frames. The differences between the fractional pixel coordinates from the 1x and 5x reconstructions for these stars are shown in Figure 1. There is no indication of a systematic bias in the 1x fractional pixel coordinates, relative to the presumably accurate 5x coordinates, giving us somewhat more confidence in the error estimates quoted in Table 1.

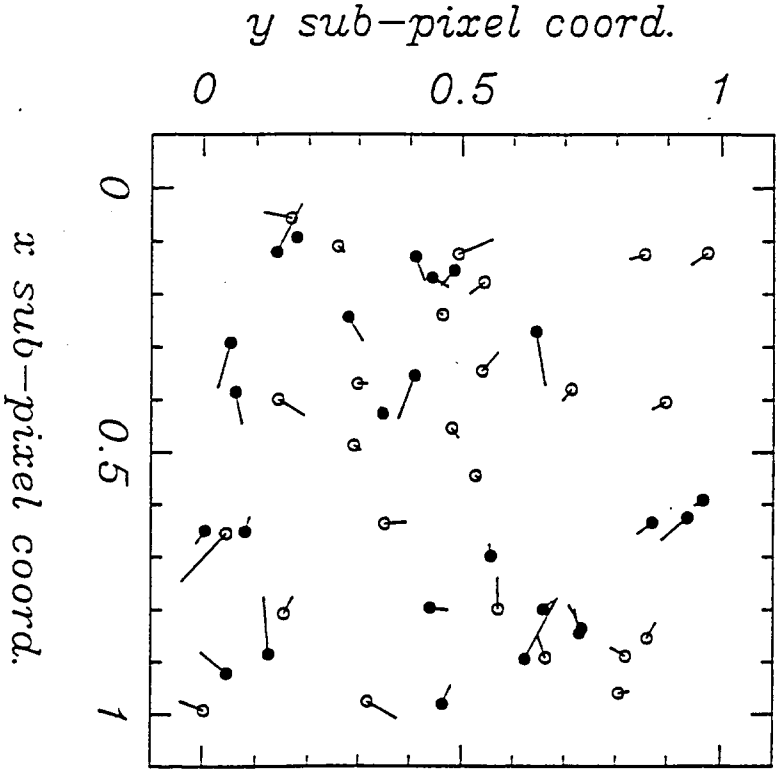

Figure 1: Fractional pixel coordinates based on the 5x subsampled reconstructions on the F555W (filled circles) and F785LP (open circles) frames. The vectors indicate the difference between the 5x and 1x sub-pixel positions. There is no evidence for a systematic bias toward the center of the pixel in the 1x data. The pixel size is 0.043 arcseconds.

In an attempt to determine just how the image coordinates "converge" from their 1x to their 5x values, linear transformations of the Nx positions were transformed into the 5x positions. The standard error of each transformation is plotted in Figure 2. Unexpectedly, the error does not decrease monotonically but is a minimum for the 3x transformation, (the error at 5x has been artificially plotted as 0.0). If instead the transformations are performed into the 4x coordinates, also shown in Figure 2, the minimum appears for the 2x data! Clearly there is an artifact of the subsampling/ reconstruction process rearing its ugly head here. This effect is currently being explored. It is encouraging to see, however, especially in the F555W data, a quick convergence at small subsampling factor.

The Gaussian centering algorithm performs better as the number of iterations through the reconstruction process increases, not surprisingly. Positions based on 0 raw, 20, 40, 60, and 80 iterations were transformed into positions derived from a 100 iteration reconstruction of the 4x subsampled frame. The transformation standard

errors are plotted in Figure 3. The 0 iteration, raw, results are deflateddue to the fact that only the 11 brightest stars centered in the raw frame reduction, whereas the processed frames centered from 30 to 40 stars.

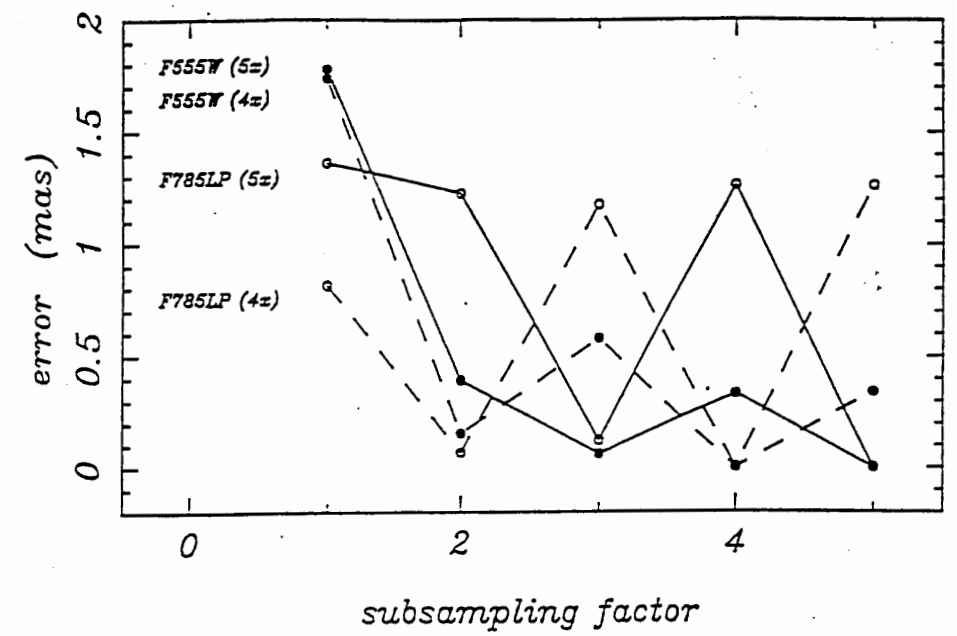

Figure 2: Single-coordinate standard errors of linear transformations between the Nx reconstructed positions and the 5x based positions (solid line) and the same for transformations between the Nx and 4x positions (dashed line). The 5x into 5x and 4x into 4x errors have been artificially set to 0.

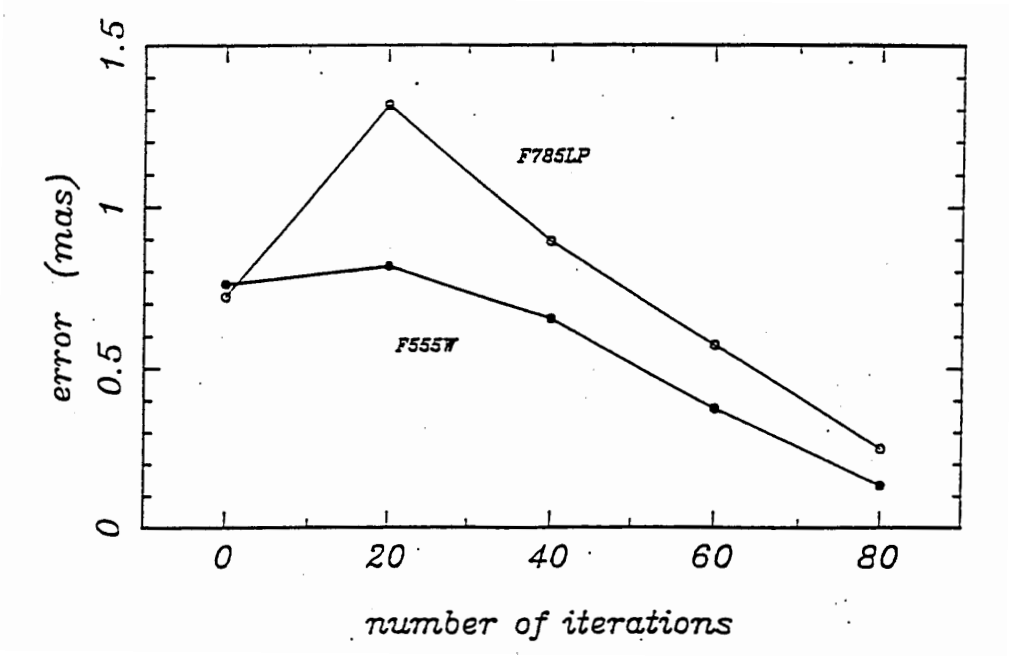

Figure 3: Single-coordinate transformation errors for the 4x based reconstructed frame as a function of the number of iterations through the reconstruction routine. The positions are transformed (linear spatial terms) into those derived from the 100 iteration frame.

VI. Summary

- image reconstruction allows more robust image centering, (in terms of number of stars centered and their magnitude range)
- preliminary indications are that positions based on reconstructed images are of higher accuracy, approaching 11 mas for well-exposed images
- subsampling before reconstruction qualitatively improves the final image and aids the centering routine in detecting faint images, although possible systematics introduced by the reconstruction process require further study
- a repeatability of 0.6 mas has been found for well-exposed images, although only for consecutive *HST* orbits with nearly identical pointing
- the important problem of modeling the distortions across the field of the PC remains to be addressed

References

Girard and van Altena, 1990, BAAS 22, 1277
Nez and Llacer, 1990 Astrophys. and Space Sci. 171, 341